

## Supporting material of the paper

### Large synthesis of in situ field measurements of the size distribution of mineral dust aerosols across their lifecycle

Paola Formenti and Claudia Di Biagio

Université de Paris and Univ Paris Est Creteil, CNRS, LISA, F-75013 Paris, France

**Table S1. Listing of the observations contributing to the in situ dataset.** Summary of available field studies data from past field campaigns. Data are categorized as SOURCE (emission and <1 days of transport), MRT or Mid-Range Transport (1 to 4 days of transport), and LRT or Long-Range Transport (> 4 days of transport), respectively. Data are ordered chronologically. In the Table the “Diameter measured” column indicates the diameter definition from the used technique. For data for which multiple instruments are used to measure the size distribution the “Diameter measured” column indicate the assumed dominant diameter definition in the considered study, usually corresponding to the technique documenting the majority of the dust size range. The “Diameter size data” column provides instead the diameter definition as reported in the size distribution data from the original paper. In this column “geometrical” means that corrections are applied in the original paper to convert the measured diameter (projected area, aerodynamic, optical) into a geometrical diameter. More details on the description of each dataset and on the different diameter definitions and their conversions to geometrical (volume-equivalent, sphere assumption) diameter are provided in Texts S3 and S4, respectively. Acronyms for the field campaign and the different instruments are reported in Texts S1 and S2, respectively.

**Table S2.** Synthesis of diameter definitions and corrections under spherical and aspherical assumptions.

**Figure S1.** Aspherical to spherical ratio ( $ASR(D_{geom})$ ) obtained at  $1.53-0.0032i$  refractive index for different OPC models as retrieved from calculations in Formenti et al. (2021) (CDP, FSSP-300, GRIMM1.109/1.129, PCASP) and at  $1.48-0.0012i$  and  $1.51.0038i$  as calculated in Huang et al. (2021) (CLIMET, WELAS) assuming tri-axial ellipsoids dust. The yellow dotted curve represents the average curve obtained by averaging the different datasets as explained in the text, smoothed over a 10-width running mean window.

**Figure S2.** Comparison of SOURCE, MRT, and LRT data for LEV1 (top), LEV2a (center), and LEV2b (bottom) analysis. As in Fig. 3 in the main manuscript, all datasets reported in this figure are normalized at the integral of 1 in the common diameter range 0.35 to 17.8  $\mu\text{m}$  and shown as mean  $\pm$  standard deviation.

**Figure S3.** Vertical distribution of the different datasets used in the present analysis for the SOURCE (black), MRT (blue), and LRT (red).

**Text S1.** Acronyms and year of field campaigns

**Text S2.** Size instrumentation generalities and acronyms

**Text S3.** Conversion formulas between diameter definitions

**Text S4.** In situ dataset description

40 **Table S1. Listing of the observations contributing to the in situ dataset.** Summary of available field studies  
41 data from past field campaigns. Data are categorized as SOURCE (emission and <1 days of transport),  
42 MRT or Mid-Range Transport (1 to 4 days of transport), and LRT or Long-Range Transport (> 4 days of  
43 transport), respectively. Data are ordered chronologically. In the Table the “Diameter measured”  
44 column indicates the diameter definition from the used technique. For data for which multiple  
45 instruments are used to measure the size distribution the “Diameter measured” column indicate the  
46 assumed dominant diameter definition in the considered study, usually corresponding to the technique  
47 documenting the majority of the dust size range. The “Diameter size data” column provides instead the  
48 diameter definition as reported in the size distribution data from the original paper. In this column  
49 “geometrical” means that corrections are applied in the original paper to convert the measured  
50 diameter (projected area, aerodynamic, optical) into a geometrical diameter. More details on the  
51 description of each dataset and on the different diameter definitions and their conversions to  
52 geometrical (volume-equivalent, sphere assumption) diameter are provided in Texts S3 and S4,  
53 respectively. Acronyms for the field campaign and the different instruments are reported in Texts S1  
54 and S2, respectively.

55

Reference	Ground/Airborne, location, field campaign acronym	Measurement technique	Diameter measured	Diameter size data	Source	MRT	LRT
Gillette et al. (1972, 1974) Gillette (1974)	Ground, Texas and Nebraska	Microscopy	Projected-area	Projected-area a	X		
Schütz (1981)	Ship-based, Atlantic Ocean	Microscopy	Projected-area	Projected-area a		X	
	Ship-based, Atlantic Ocean						X
d’Almeida (1987)	Ground, Niger	Microscopy	Projected-area	Projected-area a		X	
de Reus et al. (2000)	Airborne, Tenerife – Canary Islands, ACE2	DMPS + OPC	Optical	Geometrical		X	
Maring et al. (2000)	Ground, Izana – Canary Islands	SMPS + APS	Aerodynamic	Geometrical		X	
Formenti et al. (2001)	Ground – Brasil, CLAIRE	Chemical composition	Aerodynamic	Aerodynamic			X
Bates et al. (2002)	Ground, Indian Ocean, AEROSOLS99	DMPS+APS	Aerodynamic	Geometrical		X	
	Ground, Indian Ocean, INDOEX					X	
Maring et al. (2003)	Ground, Puerto Rico, PRIDE	SMPS+APS	Aerodynamic	Geometrical			X
Reid et al. (2003a)	Airborne, Puerto Rico, PRIDE	Microscopy	Projected-area	Projected-area a			X
Reid et al. (2003b)	Airborne, Puerto Rico, PRIDE	OPC	Optical	Optical			X
	Ground, Puerto Rico, PRIDE	Chemical composition	Aerodynamic	Geometrical			X
Clarke et al. (2004)	Airborne, Sea of Japan, ACE-Asia & TRACE-P	OPC	Optical	Optical		X	
Fratini et al. (2007)	Ground, Gobi desert	OPC	Optical / aerodynamic**	Geometrical	X		
Kobayashi et al. (2007)	Ground, Japan	Coulter multisizer	Geometrical	Geometrical		X	
						X	
Otto et al. (2007)	Airborne, Cape Verde, ACE2	DMPS + OPC	Optical	Geometrical		X	
Chou et al. (2008)	Airborne, Niger, DABEX	Microscopy	Projected-area	Projected-area a		X	
McConnell et al. (2008)	Airborne, Dakar, DODO1	OPC	Optical	Optical		X	
	Airborne, Dakar, DODO2					X	
Osborne et al. (2008)	Airborne, Niger, DABEX	OPC	Optical	Optical		X	
Rajot et al. (2008)	Ground, Niger, AMMA – Local erosion	OPC	Optical	Optical	X		
	Ground, Niger, AMMA – advection distant sources					X	
Reid et al. (2008)	Ground, Saudi Arabia, UAE2 – A	APS	Aerodynamic	Aerodynamic		X	
	Ground, Saudi Arabia, UAE2 – B					X	
Sow et al. (2009)	Ground, Niger, AMMA	OPC	Optical	Optical	X		
Wagner et al. (2009)	Airborne, Portugal, DARPO	OPC	Optical	Geometrical		X	
Weinzierl et al. (2009)	Airborne, Morocco, SAMUM1	OPC	Optical	Geometrical		X	
Muller et al. (2010)	Ground, Cape Verde, RHAMBLE	SMPS + APS	Aerodynamic	Geometrical		X	

Chen et al. (2011)	Airborne, Cape Verde/West Sahara, NAMMA	OPC + APS	Aerodynamic	Geometrical		X	
Formenti et al. (2011)	Airborne, Niger, AMMA – erosion	OPC	Optical	Geometrical		X	
	Airborne, Niger, AMMA – transport					X	
Johnson and Osborne (2011)	Airborne, West Sahara, GERBILS	OPC	Optical	Geometrical		X	
Kandler et al. (2011)	Ground, Cape Verde (Praia), SAMUM2	DMPS+APS+m icroscopy	Projected–area	Projected–area		X	
Shao et al. (2011)	Ground, Australia, JADE	OPC	Optical	Geometrical	X		
Weinzierl et al. (2011)	Airborne, Cape Verde, SAMUM2	OPC	Optical	Geometrical		X	
Jung et al. (2013)	Barbados, BACEX	OPC	Optical	Optical			X
Ryder et al. (2013a, 2013b)	Airborne, West Sahara and Canary Islands, FENNEC – fresh dust category	OPC + OAP	Optical	Geometrical	X		
	Airborne, West Sahara and Canary Islands, FENNEC – aged dust category					X	
	Airborne, West Sahara and Canary Islands, FENNEC – SAL dust category					X	
Rosenberg et al. (2014)	Airborne, central Sahara, FENNEC	OPC + OAP	Optical	Geometrical	X		
Meloni et al. (2015)	Airborne, Lampedusa, GAMARF	OPC	Optical	Optical		X	
Denjean et al. (2016a)	Ground, Puerto Rico, DUST-ATTACK	SMPS + OPC	Optical	Geometrical			X
Denjean et al. (2016b)	Airborne, Mediterranean sea, ChArMEx/ADRI-MED	SMPS + OPC	Optical	Geometrical		X	
Struckmeier et al. (2016)	Ground, Rome, DIAPASON2013–2014	APS	Aerodynamic	Aerodynamic		X	
Weinzierl et al. (2017)	Airborne, Cape Verde, SALTRACE	CPC + OPC	Optical	Geometrical		X	
	Airborne, Barbados, SALTRACE						X
Moran Zuoloaga et al. (2018)	Ground, Amazonian forest, GoAMAZON	OPC	Optical	Optical			X
Renard et al. (2018)	Airborne, Mediterranean sea, ChArMEx/ADRI-MED	OPC	Optical	Geometrical		X	
Ryder et al. (2018)	Airborne, Cape Verde, AER-D	OPC + OAP	Optical	Geometrical		X	
Huang et al. (2019)	Ground, California	OPC	Optical	Geometrical	X		
Khalfallah et al. (2020)	Ground, Dar Dhaoui, Tunisia, Wind-O-V's	OPC	Optical	Geometrical	X		
González-Flórez et al. (2023)	Ground, Morocco, FRAGMENT	OPC	Optical	Geometrical	X		

56 \*\* for Fratini et al. (2007) we used the dataset as retrieved by Kok et al. (2017) who converted the dataset  
57 as aerodynamic diameter.

58

59 **Table S2.** Synthesis of diameter definitions and corrections under spherical and aspherical assumptions.

60

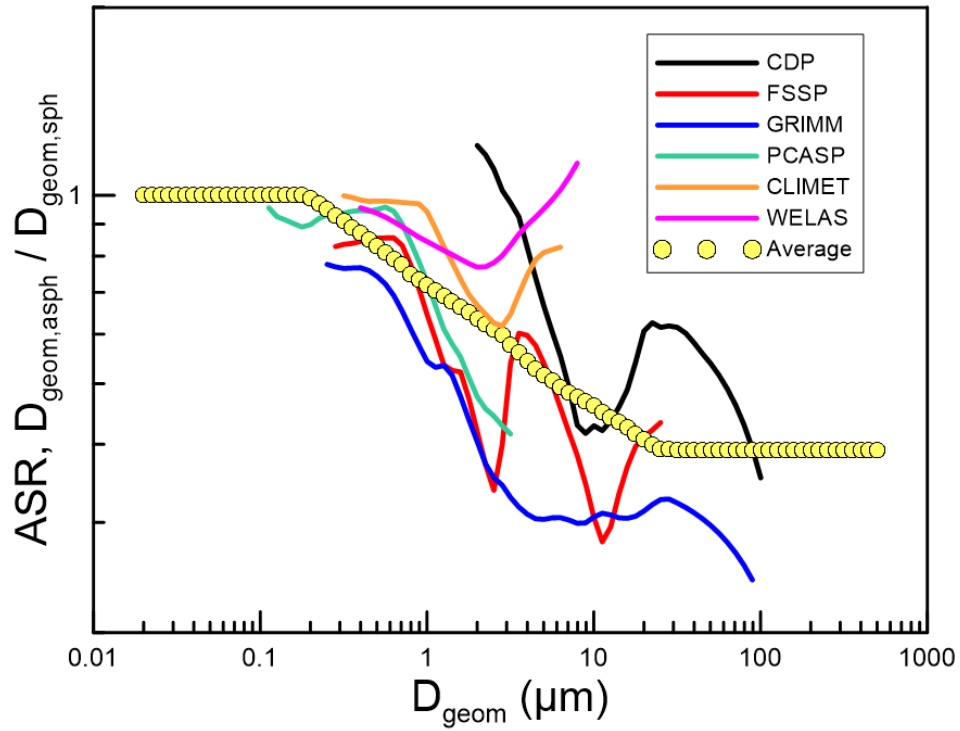
Diameter definition (technique)	Correction under spherical assumption	Correction under aspherical assumption
Geometrical (i.e., coulter counter), $D_{\text{geom}}$	$D_{\text{geom,sph}} = D_{\text{geom}}$	$D_{\text{geom,asph}} = D_{\text{geom}}$
Projected-area (i.e., microscopy), $D_{\text{area}}$	$D_{\text{geom,sph}} = D_{\text{area}}$	$D_{\text{geom,asph}} = D_{\text{area}}/1.56$
Aerodynamic (i.e., APS or cascade impactor), $D_{\text{aerod}}$	$D_{\text{geom,sph}} = D_{\text{aerod}}/1.58$	$D_{\text{geom,asph}} = D_{\text{aerod}}/1.45$
Mobility (i.e., DMPD or SMPS), $D_m$	$D_{\text{geom,sph}} = D_m/1.0$	$D_{\text{geom,asph}} = D_m/1.19$
Optical (i.e., OPC), $D_{\text{opt}}$	$D_{\text{geom,sph}} = D_{\text{opt}}$ (Mie theory)	$D_{\text{geom,asph}} = D_{\text{geom,sph}} \cdot \text{ASR}(D_{\text{geom,sph}})$

61

62

63 **Figure S1.** Aspherical to spherical ratio ( $ASR(D_{geom})$ ) obtained at  $1.53-0.0032i$  refractive index for  
64 different OPC models as retrieved from calculations in Formenti et al. (2021) (CDP, FSSP-300,  
65 GRIMM1.109/1.129, PCASP) and at  $1.48-0.0012i$  and  $1.51.0038i$  as calculated in Huang et al. (2021)  
66 (CLIMET, WELAS) assuming tri-axial ellipsoids dust. The yellow dotted curve represents the average  
67 curve obtained by averaging the different datasets as explained in the text, smoothed over a 10-width  
68 running mean window.

69



70

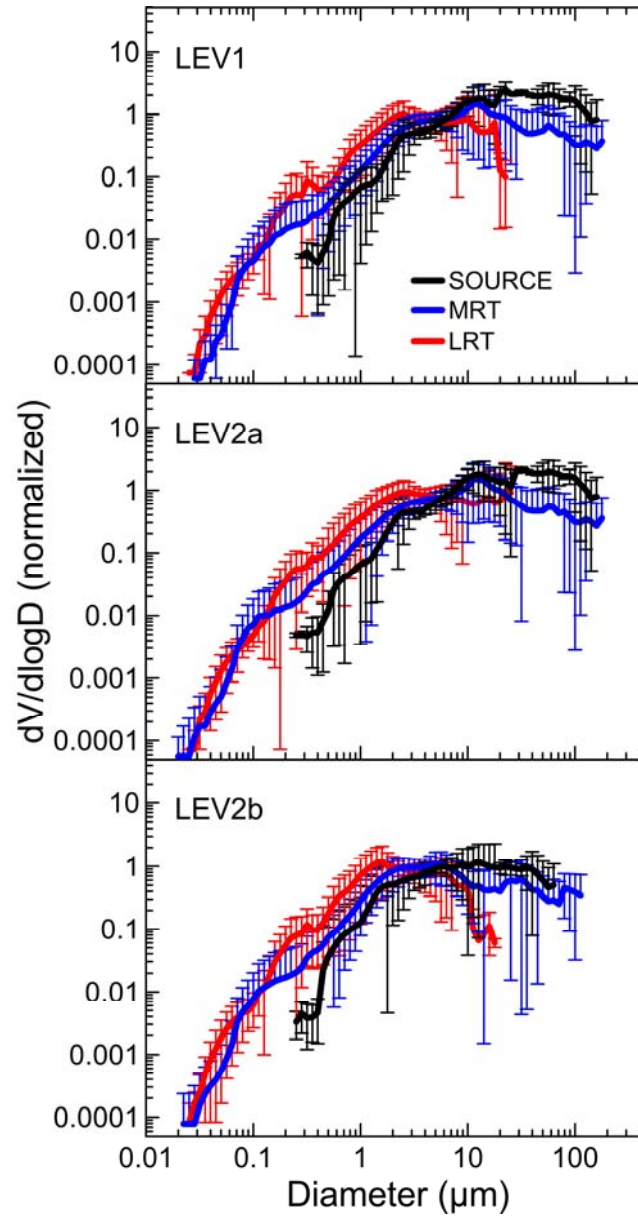
71

72

73 **Figure S2.** Comparison of SOURCE, MRT, and LRT data for LEV1 (top), LEV2a (center), and LEV2b (bottom)  
74 analysis. As in Fig. 3 in the main manuscript, all datasets reported in this figure are normalized at the  
75 integral of 1 in the common diameter range 0.35 to 17.8  $\mu\text{m}$  and shown as mean  $\pm$  standard deviation.

76

77



78

79

80

81

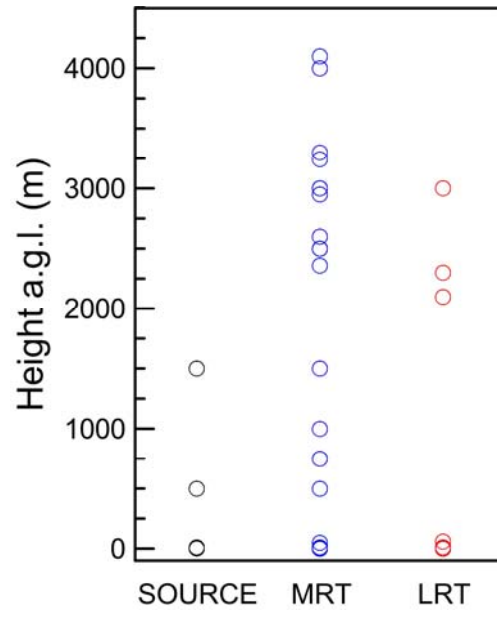
82

83

84

85 **Figure S3.** Vertical distribution of the different datasets used in the present analysis for the SOURCE  
86 (black), MRT (blue), and LRT (red).

87  
88  
89



90

91 **Text S1. Acronyms and year of field campaigns**

92 ACE2= second Aerosol Characterization Experiment (1997)

93 ACE-ASIA = Asian Aerosol Characterization Experiment (2001)

94 ADRIMED = Aerosol Direct Radiative Impact on the regional climate in the MEDiterranean region (2013)

95 AER-D = AERosol Properties – Dust (2015)

96 AMMA = African Monsoon Multidisciplinary Analysis (2006)

97 ATTO = Amazon Tall Tower Observatory (2011 –)

98 BACEX = Barbados Aerosol Cloud Experiment (2010)

99 CLAIRE-98= Cooperative LBA Airborne Regional Experiment (1998)

100 DABEX = Dust And Biomass-burning Experiment (2006)

101 DARPO = Desert AeRosol over Portugal (2006)

102 DIAPASON = Desert-dust Impact on Air quality through model-Predictions and Advanced Sensors  
103 ObservatioNs (2013)

104 DODO = Dust Outflow and Deposition to the Oceans (DODO1, February 2006; DODO2, August 2006)

105 Dust-Attack = DUST Aging and Transport from Africa to the Caribbean (2012)

106 FENNEC = The Saharan Climate System (2010–2012)

107 FRAGMENT = FRontiers in dust minerAloGical coMposition and its Effects upoN climate (2019)

108 GAMARF = Ground-based and Airborne Measurements of the Aerosol Radiative Forcing (2008)

109 GERBILS = Geostationary Earth Radiation Budget Intercomparisons of Longwave and Short-wave  
110 radiation (2007)

111 GoAmazon = Green Ocean Amazon Experiment (2014–2015)

112 INDOEX= Indian Ocean Experiment (1999)

113 JADE = Japanese Australian Dust Experiment (2006)

114 NAMMA = NASA African Monsoon Multidisciplinary Analysis (2006)

115 PRIDE= Puerto Rico Dust Experiment (2003)

116 RHaMBLe = Reactive Halogens in the Marine Boundary Layer (2007)

117 SALTRACE = Saharan Aerosol Long-range Transport and Aerosol-Cloud-Interaction Experiment (2016)

118 SAMUM = Saharan Mineral Dust Experiment (SAMUM1, 2006; SAMUM2, 2008)

119 TRACE-P= Transport and Chemical Evolution over the Pacific (2001)

120 UAE2 = United Arab Emirates Unified Aerosol Experiment (2003)

121 WIND-O-V's= WIND erOsion in presence of sparse Vegetation (2017)

122



## 123 Text S2. Size instrumentation generalities and acronyms

124 Documenting the dust size distribution is an experimental challenge. There is no unique in situ  
125 instrument covering the natural dynamical range of the mineral dust size and concentration, which can  
126 only be represented by a combination of instruments based on different intrinsic particle properties  
127 such as density, electrical charge, shape and composition (e.g., Reid et al., 2003a; Formenti et al., 2011;  
128 Wendisch and Brenguier, 2013; Mahowald et al., 2014). Light scattering techniques used by optical  
129 particle counters (OPC) provide with sizing between approximately 300 nm to 100  $\mu\text{m}$  as optical  
130 equivalent diameter referring to a sphere of given refractive index, which scatters the same amount of  
131 radiation into a given solid angle as the dust particles would do (e.g., Reid et al., 2003b; Osborne et al.,  
132 2008; Formenti et al., 2011; Ryder et al., 2013a; Weinzierl et al., 2017). Microscopy sizing methods, also  
133 providing with a large size range, are based on particle collection by filtration or impaction followed by  
134 individual particle characterization by transmission (TEM) and/or scanning electron microscopy (SEM)  
135 techniques (e.g., Reid et al., 2003b; Kandler et al., 2007; 2009; Chou et al., 2007; McConnell et al., 2008;  
136 Ryder et al., 2018). Microscopy provides information on the geometry of projected area particles.  
137 Optical array probes (OAP) can be used to measure in situ the geometry of particles and providing  
138 two-dimensional projections of them (Ryder et al., 2013; 2018). Techniques based on the Coulter  
139 principle can be also used to size insoluble particles suspended in a conductive liquid, providing the  
140 geometrical (volume-equivalent) diameter (e.g., Kobayashi et al., 2007). The submicron fraction can be  
141 sized in terms of the electrical mobility diameter of a charged particle moving in a static electric field, as  
142 done by the Differential or Scanning Mobility Particle Sizer (DMPS, SMPS) (e.g., Muller et al., 2010;  
143 Denjean et al., 2016a, 2016b). Aerodynamic particle sizers (APS), measuring the diameter of a sphere of  
144 unit density having the same terminal velocity in an accelerated airflow as the irregularly shaped dust  
145 particles e.g., (Maring et al., 2003; Reid et al., 2008; Chen et al., 2011). The mass size distribution is  
146 measured by multi-stage filtration or impaction sampling coupled with gravimetric or chemical analysis  
147 (e.g., Formenti et al., 2001; Reid et al., 2003b).

148 When retrieving the size distribution of dust over the largest possible diameter range different kind of  
149 difficulties arise:

150 1/ the first one is related to the fact of combining instruments measuring different diameters and the  
151 combination is far from being without ambiguity and subject to analysis evaluations and choices;

152 2/ the second one is related to the size-dependent sampling biases that can affect the measurements,  
153 both in the fine and the coarse fractions, and in particular due to the mass inertia of larger particles  
154 which are lost in bends and long tubes at the entrance of the instruments (Wendisch and Brenguier,  
155 2013). Largest biases are expected in airborne data from research aircraft due to the lowered sampling  
156 efficiencies at low pressure and high aircraft speed (Wendisch and Brenguier, 2013; Sanchez-Marroquin  
157 et al., 2019).

158 In the following we summarize the techniques and spell the acronyms of the different instruments  
159 considered in the literature, classified by classes of instruments providing different definitions of the  
160 measured diameter. For OPC; the most used instruments for dust size measurements, details on the  
161 nominal diameter range and operating wavelength for each instrument type are reported.

162 Geometrical diameter (volume-equivalent)

163     o Coulter counter

164 Projected-area diameter

165     o Microscopy

166         o SEM= Scanning Electron Microscopy

167         o TEM = Transmission Electron Microscopy

168     o OAP = Optical Array Probe

169         o CIP = Cloud Imaging Probe

- 170 Aerodynamic diameter
- 171     o APS = Aerodynamic Particle Sizer
- 172     o Multi-stage filtration and chemical analyses
- 173 Mobility diameter
- 174     o DMPS=Differential Mobility Particle Sizer
- 175     o SMPS= Scanning Mobility Particle Sizer
- 176 Optical diameter
- 177     o OPC= Optical Particle Counter
- 178     o CAS = Cloud and Aerosol Spectrometer, nominal diameter range 0.6–50  $\mu\text{m}$ , operating
- 179         wavelength 680 nm
- 180     o CDP = Cloud Droplet Probe, nominal diameter range 0.3 to 50  $\mu\text{m}$ , operating wavelength 658 nm
- 181     o CLIMET CI-3100= nominal diameter range 0.26–7.0  $\mu\text{m}$ , operating wavelength not found
- 182     o FIDAS 200S= nominal diameter range 0.2–19.1  $\mu\text{m}$ , polychromatic un-polarized LED light source
- 183     o FSSP-100= Forward Scattering Spectrometer Probe, nominal diameter range 0.5–47  $\mu\text{m}$ ,
- 184         operating wavelength 632.8 nm
- 185     o FSSP-300= Forward Scattering Spectrometer Probe, nominal diameter range 0.275–20.5  $\mu\text{m}$ ,
- 186         operating wavelength 632.8 nm
- 187     o GRIMM 1.108= nominal diameter range 0.3–20  $\mu\text{m}$ , operating wavelength 780 nm
- 188     o GRIMM 1.109/1.129= nominal diameter range 0.25–32  $\mu\text{m}$ , operating wavelength 655 nm
- 189     o LAS-X = nominal diameter range 0.12–7.5  $\mu\text{m}$ , operating wavelength 630 nm
- 190     o LOAC= Light Optical Aerosol Counter, nominal diameter range 0.2–100  $\mu\text{m}$ . operating wavelength
- 191     o Opc MetOne = nominal diameter range 0.49–10.0  $\mu\text{m}$ , operating wavelength 589 nm
- 192     o OPC YGK Corp. = nominal diameter range 0.3–7.0  $\mu\text{m}$ , operating wavelength 780 nm
- 193     o OPS (model 3330= = Optical Particle Sizer, nominal diameter range 0.3–10  $\mu\text{m}$ , operating
- 194         wavelength
- 195     o PCASP = Passive Cavity Aerosol Spectrometer Probe, nominal diameter range 0.1–3  $\mu\text{m}$ , operating
- 196         wavelength 632.8 nm
- 197     o SID = Small Ice Detector, nominal diameter range 2–60  $\mu\text{m}$ , operating wavelength 532 nm
- 198     o USHAS= Ultra High Sensitivity Aerosol Spectrometer, nominal diameter range 0.04–1.0  $\mu\text{m}$ ,
- 199         operating wavelength 1054 nm
- 200     o WELAS = nominal diameter range 0.3–10  $\mu\text{m}$ , operating wavelength 440 nm
- 201

### 202 Text S3. Conversion formulas between diameter definitions

203 For each diameter type definition this section discusses the treatment applied to convert data into a  
204 common geometrical (volume–equivalent) diameter definition both under the assumption of spherical  
205 and aspherical particles, as then used to convert data into LEV2a and LEV2b as discussed in the main  
206 text and following details in Text S4. The treatment discussed here follows the theory and the treatment  
207 proposed and discussed in the literature (e.g., Hinds, 1999, De Carlo et al., 2004 ; Mahowald et al., 2014;  
208 Huang et al., 2020, 2021; Formenti et al., 2021).

209 1/ *geometrical diameter* (or *volume–equivalent diameter*),  $D_{geo}$ , is defined as the diameter of a sphere  
210 having the same volume as the irregularly–shaped particle. The geometrical diameter is the parameter  
211 usually applied in climate models to refer to aerosol particles and it is the target reference diameter in  
212 this work. As discussed in Text S2 it can be measured by coulter counters.

213 2/ *projected–area diameter*,  $D_{area}$ , is the diameter of a circle having the same area as the dust particle  
214 projected in a two–dimensional image. It is obtained mostly from optical and electron microscopy,  
215 which is a diffused technique to size aerosol particles in atmospheric sciences (e.g., Gillette et al., 1972 ;  
216 Reid et al., 2003 ; Chou et al., 2008). The microscopy techniques has the advantage of providing image  
217 of the particle and to estimate its size directly from the particle visualization, but that shows multiple  
218 disadvantages, such as i/ to characterize only two particle’s dimensions, therefore requiring  
219 assumptions on the third one, ii/ to be highly time consuming and iii/ to have low spatio–temporal  
220 resolution since a minimum integration time is required to collect particles on filters to observe in  
221 microscopy. For spherical particles  $D_{area}$  is equal to  $D_{geom}$ . For aspherical dust the  $D_{area}$  diameter should  
222 be corrected to take into account deviation from sphericity. Following Huang et al. (2021) the relation  
223 between projected–area and geometrical diameter can be written as:

$$224 \quad D_{area} = D_{geom} \frac{\sqrt[6]{AR}}{\sqrt[3]{HWR}} \quad \text{Eq. S1}$$

225 where the aspect ratio (AR) and height–to–width–ratio (HWR) are the two parameters used to quantify  
226 particle asphericity for dust approximated as tri–axial ellipsoids. Huang et al. (2020) compiled global AR  
227 and HWR and found that both parameters deviate from unity and seem to be size independent and  
228 being lognormally distributed. They determine a median globally averaged value of  $1.7 \pm 0.03$  for AR  
229 and  $0.40 \pm 0.07$  for HWR. For aspherical dust, based on the application of Eq. (S1) and applying a Monte  
230 Carlo simulation taking into account the global distribution of AR and HWR, Huang et al. (2021) derived  
231 a global average conversion factor of 1.56 to convert  $D_{area}$  into a  $D_{geom}$  ( $D_{geom} = D_{area} / 1.56$ ).

232 3/ *aerodynamic diameter*,  $D_{aerod}$ , is the diameter of a spherical particle with density of  $1 \text{ g cm}^{-3}$  having  
233 the same aerodynamic resistance as the investigated aerosol. This diameter is measured by an  
234 instrument called aerodynamic particle sizer (APS). Also the cascade impactors measure integrated  
235 mass as a function of aerodynamic diameter since  $D_{aerod}$  is used to classify impactor stages cut off  
236 diameters. In the continuum regime (i.e. when a gas can be thought to be as a continuous fluid in flow  
237 around the particle, represented by the Knudsen number  $Kn \ll 1$ ) the aerodynamic diameter can be  
238 converted into a geometrical diameter by the knowledge of the particle density and the dynamic shape  
239 factor  $\chi$  in order to account for the dynamic conditions of sampled particles (De Carlo et al. 2004). The  
240 dynamic shape factor is the ratio of the aerodynamic resistance exerted on an aspherical particle to the  
241 resistance that would be exerted on a spherical particle with equal volume than the particle under  
242 consideration (Hinds, 1999). The relation linking the aerodynamic and the geometric diameter can be  
243 written as:

$$244 \quad D_{aerod} = D_{geom} \sqrt{\frac{\rho_{dust}}{\chi \rho_0}} \quad \text{Eq. S2}$$

245 where  $\rho_{\text{dust}}$  is the density of dust aerosols (assumed to be  $2.5 \text{ g cm}^{-3}$ , chosen at the mean of the range  
 246 of desert dust densities as reported in the literature, i.e.  $2.1\text{--}2.75 \text{ g cm}^{-3}$  (i.e. Maring et al., 2000; Reid  
 247 et al., 2003a; Fratini et al., 2007).) and  $\rho_0$  is the standard density ( $1.0 \text{ g cm}^{-3}$ ). For spherical dust, the  
 248 application of Eq. (S2) to a shape factor of 1 result in a conversion factor of 1.58 to correct the  $D_{\text{aerod}}$   
 249 into a  $D_{\text{geom}}$  ( $D_{\text{geom}} = D_{\text{aerod}} / 1.58$ ). For aspherical dust approximated as tri-axial ellipsoids, Huang et al.  
 250 (2021) applied the global AR and HWR compiled in Huang et al. (2020) to calculate the dynamic shape  
 251 factor for dust aerosols and used these factors to determine a size-invariant conversion factor of 1.45  
 252 that allows to transform the aerodynamic into the geometric diameter based on Eq. (S2) ( $D_{\text{geom}} = D_{\text{aerod}}$   
 253  $/1.45$ ).

254 4/ *electrical modibility diameter*,  $D_{\text{mob}}$ , the diameter of a sphere with the same migration velocity in a  
 255 constant electric field as the particle of interest. This diameter is what is measured by the DMPS or SMPS  
 256 and can be converted into a geometrical diameter based on the knowledge of the dynamical shape  
 257 factor  $\chi$  as:

$$258 \quad D_{\text{geom}} = \frac{D_m}{\chi} \quad \text{Eq. S3}$$

259 For spherical dust, a shape factor of 1 result in an equality between  $D_{\text{mob}}$  and  $D_{\text{geom}}$ . For aspherical dust  
 260 approximated as tri-axial ellipsoids, a global mean shape factor of 1.19 is estimated by Huang et al.  
 261 (2021).

262 5/ *optical diameter*,  $D_{\text{opt}}$ , the diameter of an aerosol showing the same intensity of scattered light than  
 263 the dust aerosols. The optical diameter is usually measured by means of optical particle counters (OPCs),  
 264 recording the scattered-light intensity over a specific angle range and associating a particle size based  
 265 on the knowledge or assumption of the index of refraction of the particle under investigation. Complex  
 266 refractive index assumptions and the use of optical theories adapted to aerosol shape are used to  
 267 associate a scattering intensity to a particle size, therefore allowing to convert the optical diameter into  
 268 a geometrical diameter. In this study we take advantage of the database developed by Formenti et al.  
 269 (2021) who evaluated size-dependent correction factors for dust under both the assumption of  
 270 sphericity and non sphericity and for varying refractive index for various OPC models (CDP-300,  
 271 FSSP-300, GRIMM1.129/1.109, and PCASP-100). The corrections factor by Formenti et al. (2021) for  
 272 spherical dust and assuming a refractive index of  $1.53\text{--}0.003i$  in the visible (value that is at the average  
 273 of the dust global values reported in Di Biagio et al. 2019) are applied to correct the different datasets.  
 274 For the GRIMM 1.108 OPC model, for which the conversion was not provided in Formenti et al. (2021),  
 275 the conversion in Formenti et al. (2011) for the refractive index of  $1.53\text{--}0.002i$  calculated under  
 276 spherical assumption is considered. In order to be applied in the present study the  $D_{\text{opt}}$  to  $D_{\text{geom}}$   
 277 conversion factors are recalculated at the interpolation diameters used for LEV1 to LEV2b data. For  
 278 OPCs models as listed in Text S2 and not treated in the Formenti et al. (2011) and (2021) work, the  
 279 correction corresponding to the most similar OPC model (operating wavelength, sensing angles) within  
 280 those in Formenti et al. (2011) or (2021) is used. Specific assumptions are detailed in Text S4 for each  
 281 dataset involved in the specific case.

282 To take into account for aspherical effects in OPCs corrections, the  $D_{\text{opt}}$  to  $D_{\text{geom}}$  spherical and aspherical  
 283 calculations in Formenti et al. (2021) and Huang et al. (2021) are used. These studies report for different  
 284 OPCs the optical to geometrical diameter conversion factors both in the assumption of spherical  
 285 homogeneous particles ( $(D_{\text{geom}})_{\text{spherical}}$ ) and tri-ellipsoids dust ( $(D_{\text{geom}})_{\text{aspherical}}$ ). For the calculations the  
 286 refractive index of  $1.53\text{--}0.0032i$  is used in Formenti et al. (2021) for CDP, FSSP, GRIMM and PCASP OPCS  
 287 considered here, whereas the refractive index values of  $1.48\text{--}0.0012i$  and  $1.51\text{--}0.0038i$  are used in  
 288 Huang et al. (2021) for the CLIMET and the WELAS, respectively. The size-dependent aspherical to  
 289 spherical ratio ( $\text{ASR}(D_{\text{geom}})$ ) correction function,  $\text{ASR}(D_{\text{geom}}) = (D_{\text{geom}})_{\text{aspherical}} / (D_{\text{geom}})_{\text{spherical}}$ , obtained by  
 290 averaging the ASR function obtained for the different OPC models is shown in Figure S1. The ASR  
 291 function represent the change in optical to geometrical correction when aspherical dust is assumed in  
 292 spite of spherical dust. The average  $\text{ASR}(D_{\text{geom}})$  function is taken constant at the value of 1 below 0.2

293  $\mu\text{m}$ , when no single OPC data are available for the ASR evaluation, and at the value of 0.39 above 30  $\mu\text{m}$   
294 diameter. The 0.39 value is the average obtained for between 20 and 30  $\mu\text{m}$  diameter when at least  
295 three OPCs ASR datasets are available for averaging. The  $\text{ASR}(D_{\text{geom}})$  function is then used to include the  
296 effect of asphericity in OPCs data correction, as discussed in Text S4.

297 In this study we decided to define a common  $\text{ASR}(D_{\text{geom}})$  function for all OPCs instead of defining a  
298 different one for different instrument models. This is due for two main reasons: 1/ not all OPC models  
299 used from in situ studies have specific  $\text{ASR}(D_{\text{geom}})$  documented from Formenti et al., (2021), Huang et  
300 al. (2021) or their study; 2/ several datasets considered here combine several OPCs to get their final  
301 reported size distribution and unknown information are given on how this merging is done, therefore it  
302 is unknown how to combine different  $\text{ASR}(D_{\text{geom}})$  correction functions in these cases. Given the spread  
303 in the  $\text{ASR}(D_{\text{geom}})$  functions for the different models, it is clear that the approach of using a common  
304 average ASR is over simplistic. However, and also given the heterogeneity of the dataset ensemble, this  
305 treatment allows to provide a global evaluation of for asphericity effects in the dataset ensemble.  
306

#### 307 Text S4. In situ dataset description

308 The following text describe the in situ datasets included in the present study and ordered  
309 chronologically, providing brief schematic context about the field campaigns and experiments that lead  
310 to size data measurements and the relevant technical details about instrumentation and data analysis  
311 in the original papers. This dataset description is complementary to other size dataset descriptions  
312 already provided in other studies and considering part of the same datasets used here (i.e., Kok et al.,  
313 2017; Adebisi et al., 2020). Specific assumptions for the data treatment are also provided for the  
314 datasets concerned in order to complete the data analysis description in Texts S3 and and in the main  
315 manuscript in Sect. 2.2 and 2.3 . Each dataset start with a three–field indication of the techniques used  
316 to measure size (microscopy, OPC, DMPS, DMPS+APS, ...), the indication of where the data have been  
317 acquired (ground–based or airborne), and the diameter definition as provided in the original  
318 publications. These information (reported in blue character here) are schematically synthetized in Table  
319 S1. For each dataset we also indicate clearly how the data are retrieved (contact with author, data from  
320 repository, digitalization, ..) and in which format they are expressed in the original paper. For datasets  
321 relying on multiples instruments and for which a choice on the main “dominant” instrument is done for  
322 converting to LEV2a and/or LEV2b data (see discussion in Sect. 2.2, 2.3, 2.4 in the main manuscript) we  
323 also add specification in the text of which is the main instrument considered in our analysis for data  
324 corrections. Error bars for each dataset are either the values provided in the original dataset or the  
325 variability of averaged data, when reported. When not reported, but possible, we calculate the average  
326 and standard deviation of multiple datasets. Otherwise, error bars are not reported.

327 It is worth to mention that further observations of size distribution for dust at source have been also  
328 found in the literature but not considered in the present analysis, including the work by (Kandler et al.,  
329 2009) during the SAMUM–1 campaign, and the observations by Schutz and Janicke (1974), Schutz  
330 (1981), D’Almeida (1987), Gillette and Nagamoto (1993), and Sviridenkov et al. (1993) in the Sahara, the  
331 Sahel, and Tadjikistan. These data are not considered in the main analysis mainly because of the lack of  
332 detailed information on the techniques or data acquisition and treatment, preventing from a clear  
333 assessment of their quality and/or classification, whereas for the Kandler et al. (2009) dataset acquired  
334 close to source regions in Morocco, the dataset was reported to be contaminated by very large saltation  
335 and sand–blasting grains from the soil.

336 The datasets considered in the present study are listed in the following.

- 337 ▪ **(Gillette et al., 1972, 1974a) and Gillette (1974):** [microscopy, ground–based, projected–area](#)  
338 [diameter](#). These authors reported first field measurements of the size–resolved vertical dust flux  
339 based on measurements they performed on one sandy loam, two fine sand, and two loamy fine sand  
340 soils. Observations were in Texas and Nebraska and included a range of wind speeds. Measurements  
341 were performed using a two single–stage impactors installed at heights of 1.5 and 6 m above the  
342 ground level. The aerosols collected on filters were analyzed by optical microscopy technique to  
343 retrieve the size–resolved vertical dust flux between 1 and 20  $\mu\text{m}$  diameter range. Data from Gillette  
344 studies were treated and synthetized in Kok et al. (2017) and we assume the same dataset as Kok et  
345 al. in the present analysis. Original data are expressed as size–resolved aerosol fluxes ( $\text{dN cm}^{-2} \text{s}^{-1}$ )  
346 In this study we take the  $\text{dV}/\text{dlogD}$  data normalized at the integral of 1 between 0.2 and 20  $\mu\text{m}$  as  
347 published in Kok et al. (2017). Data are obtained from J. Kok (personal communication).
- 348 ▪ **(Schütz et al., 1981):** [microscopy, ship–based, projected–area diameter](#). They reported size  
349 distribution data for dust close to the source, labelled as Sahara and corresponding to SAL  
350 observations, and data for transport distances of 1000, 2000, and 5000 km obtained from  
351 surface–level measurements from the German vessel Meteor while crossing the Atlantic Ocean at a  
352 latitude of about 15°N. In this study we used size distribution data for transport of 1000 km as  
353 representative of the MRT conditions, and data for 5000 km as representative of LRT. Geographical  
354 coordinates were defined arbitrarily based on information from the paper and transport distances.

355 Original data are reported as  $dV/d\log R$ . Data are digitalized from the original publication in their  
356 Figure 14.5).

357 ▪ **(d'Almeida, 1987):** [microscopy, ground-based, projected-area diameter](#). Aerosol particles were  
358 collected on filter substrate, then dissolved in an organic liquid to put them in suspensions, and  
359 further counted with scanning electron microscopy (d'Almeida and Schütz, 1983). The procedure  
360 avoided charging effects on the sample surface and data were corrected to account for the filter  
361 collection efficiency. Measurements were taken at three sites in Senegal, Mali and Niger between  
362 February–March 1979, and January–February 1982. Observations corresponding to sandstorm and  
363 wind carrying dust conditions are shown in their Figure 3. The wind carrying dust represents dust  
364 after 1 or 2 days after the heavy sandstorm episode. In the present study we use the wind carrying  
365 dust observations as representative of MRT conditions, whereas the sandstorm dataset was not  
366 considered because of lacking information on the age of the plume to properly identify the data as  
367 SOURCE category. Original data are reported as  $dN/d\log D$ . Data are digitalized from the original  
368 publication in their Figure 3.

369 ▪ **(de Reus et al., 2000):** [DMPS + OPC \(PCASP, FSSP-300\), airborne, geometrical diameter](#). Airborne  
370 observations of the aerosol size distribution were retrieved during the Second Aerosol  
371 Characterization Experiment (ACE 2) near Tenerife, Canary Islands, in July 1997. The size distribution  
372 of dust aerosols was measured in the submicron range by combining a DMA and a CPC from 0.02 up  
373 to 0.15  $\mu\text{m}$  and an OPC PCASP to get aerosol size between 0.11 and 3.5  $\mu\text{m}$ . The PCASP was calibrated  
374 with ammonium sulphate aerosols below 1  $\mu\text{m}$  diameter and with PSL above 1  $\mu\text{m}$ . An FSSP-300 was  
375 installed on the fuselage and measured up to 31  $\mu\text{m}$  diameter. It is reported that the FSSP is  
376 calibrated with a refractive index of 1.55–0.004i for Saharan dust aerosols. Measurements  
377 correspond to the dust aerosols measured at 4 km altitude. In our treatment we assume the OPC to  
378 be the main instrument of reference for LEV2b corrections. Original data are reported as both  
379  $dN/d\log D$ ,  $dS/d\log D$ , and  $dV/d\log D$  in their figure 4. We considered the  $dV/d\log D$  ( $\mu\text{m}^3 \text{cm}^{-3}$ ) from  
380 Figure 4c. Data are digitalized from the original publication.

381 ▪ **(Maring et al., 2000):** [SMPS+APS, ground-based, geometrical diameter](#). In their work they reported  
382 dust size distribution measurements in the free troposphere at 2360 m at Izana, Tenerife (Canary  
383 Island) in July 1995. The size distribution was derived by combining a TSI Scanning Mobility Particle  
384 Sizer (SMPS) Model 3934L sizing aerosols from 0.013 to 0.85  $\mu\text{m}$  with a TSI Aerodynamic Particle  
385 Sizer (APS) Model 3310 measuring in the range going from 0.8 up to >15  $\mu\text{m}$  aerodynamic diameter.  
386 Aerosols with diameters >0.6  $\mu\text{m}$  measured at Izana in July 1995 appeared to be almost exclusively  
387 mineral dust. Dust mass closure calculations in their study indicated that the dry dust aerosol density  
388 is 2.0  $\text{g cm}^{-3}$ , and this value was used in the original publication to convert aerodynamic to geometric  
389 diameters. In absence of further information we assume the shape factor of dust to be equal to 1 in  
390 the original data analysis. In our treatment we assume the APS to be the main instrument of  
391 reference for LEV2a and LEV2b corrections. We report here the synthesis of their data as  $dV/d\log D$   
392 peak–height normalized distribution as reported in Maring et al. (2003) in their Figure 3. Data are  
393 digitalized from the original publication.

394 ▪ **(Formenti et al., 2001):** [cascade impactor, ground-based, aerodynamic diameter](#). Measurements  
395 were acquired in Brasil at the site of Balbina during the CLAIRE-98 experiment. Mass size distribution  
396 was derived from elemental analysis of dust samples collected on a 12 stages small deposit-area  
397 low-pressure impactor (SDI) operated at 11  $\text{L min}^{-1}$ . The authors indicated that at this flow rate, the  
398 cut points were 8.5, 4.1, 2.7, 1.7, 1.1, 0.77, 0.59, 0.34, 0.23, 0.15, 0.086 and 0.045  $\mu\text{m}$  as equivalent  
399 aerodynamic diameters. At Balbina, transport of mineral dust from Africa within the NE trade winds  
400 took place without interruption from 24 to 27 March 1998, for dust originated across the Moroccan  
401 coast for trajectories arriving below 800 hPa on the 25th March. The mass size distributions  
402  $dM/d\log D$  of several elements (Al, P, S, Cl, K, Ca, V, and Zn) were reported in their Figure 11 for dust  
403 sampling on the 25 March. The size distribution of the Al element is considered here as

404 representative of dust. Original data are mass size distribution  $dM/d\log D$  as  $\text{ng m}^{-3}$ . Data were  
405 digitalized from the original paper, their Figure 11.

406 ▪ **(Bates et al., 2002): DMPS+APS, ground-based, geometrical diameter.** Aerosol number size  
407 distributions were measured aboard the Research vessel Ronald H. Brown during the Indian Ocean  
408 Experiment (INDOEX) 1999 Intensive Field Phase. Measurements combined a differential mobility  
409 particle sizer (DMPS) working on 27 size bins with midpoints diameters ranging from 0.022 to 0.9  $\mu\text{m}$   
410 and an aerodynamic particle sizer (APS), covering a size range between 0.6 and 9.6  $\mu\text{m}$  aerodynamic  
411 diameter. Taking into account inlet efficiency and instrumental corrections, it resulted that the size  
412 was measured from 0.02 to 7  $\mu\text{m}$  geometric diameter at 55% relative humidity. In doing diameter  
413 conversions the authors assumed an aerosol density of 1.33  $\text{g cm}^{-3}$  as indicated in Quinn et al. (2002).  
414 The aerosol number size distributions measured during the campaign in the Indian Ocean marine  
415 boundary layer were categorized into eight air mass source regions based on air mass back  
416 trajectories. We report here the average size distribution from their Figure 4 corresponding to the  
417 average for the SHmX Southern Hemisphere marine Extratropical air mass condition, corresponding  
418 to a transport time of up to 108 h that we associate to MRT category, and also the retrieved mineral  
419 dust data from their Figure 5 as measured during the AEROSOL99 campaign and corresponding to a  
420 dust transport of 43h. In our treatment we assume the APS to be the main instrument of reference  
421 for LEV2a and LEV2b corrections in both datasets. In absence of further information we assume the  
422 shape factor of dust to be equal to 1 in the original data analysis. Data are reported as both  $dN/d\log D$   
423 and  $dV/d\log D$  and we took the volume data as reported in their Figures 4c and 5b. Data are digitalized  
424 from the original publication.

425 ▪ **(Maring et al., 2003): SMPS+APS, ground-based, geometrical diameter.** They reported  
426 measurements of the dust size distribution measured at the sea level in Puerto Rico during PRIDE in  
427 July 2000. Size distribution measurements and setup were similar to those of Maring et al. (2000) at  
428 Izana, with the only difference that the sample inlet in Puerto Rico, which is a humid environment  
429 with often  $\text{RH} > 80\%$ , was heated so to reduce RH to values below 50%. Measurements during PRIDE  
430 confirmed, as observed at Izana in Maring et al. (2000), that aerosols with diameters  $> 0.6 \mu\text{m}$   
431 consisted of dust and sea salt, in contrast with the accumulation mode particles. A dust-dominated  
432 size distribution for PRIDE was obtained by subtracting to the campaign average the size distribution  
433 measured for periods of high sea salt concentrations based on concurrent chemical analyses. A dust  
434 mass closure calculation indicated a dry dust aerosol density of 2.0  $\text{g cm}^{-3}$ . This density was used to  
435 convert all aerodynamic to geometrical diameters. In our treatment we assume the APS to be the  
436 main instrument of reference for LEV2a and LEV2b corrections in both datasets. We report here the  
437 synthesis of the data reported from these authors as  $dV/d\log D$  peak-height normalized distribution  
438 as in their figure 3. Data are digitalized from the original publication.

439 ▪ **(Reid et al., 2003a): microscopy, airborne, projected-area diameter.** Atmospheric dust samples were  
440 collected by Piper Nvajo aircraft at various elevations in the SAL during the PRIDE field campaign in  
441 Puerto Rico in June–July 2000. The samples for single particle analysis were collected at a flow rate  
442 of 5  $\text{L min}^{-1}$  by means of a nearly isokinetic inlet with a 50% cutoff at 10  $\mu\text{m}$  for dry dust. The authors  
443 noted in the paper that anyhow some large particles up to 20  $\mu\text{m}$  in diameter could be collected,  
444 particularly at low humidity conditions. The size distribution of dust aerosols was obtained by the  
445 analysis of SEM microscopy images. Particle area and volume distributions are presented in their  
446 Figure 8 for selected dust samples. Estimated volume distributions are modelled to be lognormal,  
447 with volume median diameters (VMD) from 7 to 9  $\mu\text{m}$ , and geometrical standard deviations on the  
448 order of 1.6 to 1.8. Original data are reported as area and volume normalized distribution in their  
449 Figure 8. We consider the volume size distribution in our study and we calculated the average and  
450 standard deviation of the data reported in Figure 8 for dust in the SAL (4 datasets between the 16th  
451 and the 22 July). Data are digitalized from the original publication.

452 ▪ **(Reid et al., 2003b): 2 datasets: (cascade impactor, ground-based, geometrical diameter) && (OPC,**  
453 **airborne, optical diameter).** In their paper Reid et al. report a summary of size observations as



454 obtained during the PRIDE campaign in 2000 at Puerto Rico. Some of the data discussed in this paper  
455 were summarized elsewhere, in particular the ground based APS observations at Puerto Rico were  
456 reported in Maring et al. (2003) and the complete analysis of the airborne microscopy samples was  
457 reported by Reid et al. (2003a) and discussed just above. In this paper their reported additional data  
458 of dust size distributions recorded at Puerto Rico in July 2000 as obtained by means of cascade  
459 impactor observations at the Cabras Island site and airborne OPC data. The cascade impactor used  
460 during PRIDE was the University of Miami MOUDI system (MicroOrifice, Uniform–Deposit Impactor)  
461 collecting samples in 8 stages with 50% cut points at 22, 12, 7.6, 3.8, 2.2, 1.24, 0.71, and 0.41  $\mu\text{m}$ .  
462 One integrated 68 hour sample obtained in the period 21 to 24 July was used to determine Al, Br, Cl,  
463 Mn, Na, V, I, and K elements (neutron activation analysis, NAA). The dust mass size distribution was  
464 derived by considering as tracer the Al, and so the Al mass distribution was taken as representative  
465 of dust aerosols. The conversion between Al and dust mass was 12.5 or 8% of mass. Aerodynamic to  
466 geometrical conversion was performed assuming a conversion factor of 1.4 as the square root of the  
467 dynamic shape factor divided by particle density. Both the aerodynamic and the retrieved  
468 geometrical distributions are presented in Figure 6 of Reid et al. for the dust event of the 21–24  
469 July 2000. To note that a second cascade impactor, the Devis Rotating Drum (DRUM), was also used  
470 in Puerto Rico to derive the dust mass distribution by XRF analysis. However, since mass distribution  
471 data are only reported as a function of the aerodynamic diameter in that second case, and because  
472 the upper channel was at only 5  $\mu\text{m}$  diameter, we do not consider this further dataset in our analysis.  
473 Additional observations of the dust size distribution were reported by Reid et al. considering the  
474 airborne measurements of two OPCs (an FSSP–100 and a PCASP–100X) wing–mounted on the Navajo  
475 aircraft. The PCASP provided the dry particle size distribution (RH =35–40%), whereas the FSSP–100  
476 inferred the ambient size distribution. Both instruments were calibrated before and after the  
477 campaign with PSL particles. The number, surface and volume size distribution for five dust events  
478 in July 2000 for the OPCs are reported in their Figure 10. In the present study we consider the average  
479 and standard deviation of these observations. In our treatment we assume the FSSP–100 to be the  
480 main instrument of reference for LEV2a and LEV2b corrections for OPCs data. For LEV2a data  
481 correction we assume that the optical to geometrical conversion is the same that the one estimated  
482 for the FSSP–300 as reported in Formenti et al. (2021), despite a smaller opening receiving angle  
483 (5–13°) in the FSSP–100 model than in the FSSP–300 model (3–15°). Original data are reported as  
484 mass size distributions from the cascade impactors and as number, surface and volume size  
485 distribution for the OPCs. Data are digitalized from the original paper from their Figure 6 for cascade  
486 impactor data and from their Figure 10 for OPCs data.

487 ▪ **(Clarke et al., 2004): OPC, airborne, optical diameter.** These authors report measurements taken  
488 during the ACE–Asia and TRACE–P campaigns in the Sea of Japan (between Korea and Japan) in the  
489 spring (24 February to 10 April) of 2001. Size distribution between diameters of 0.1 and 10  $\mu\text{m}$  was  
490 measured by means of an optical particle counter (OPC, a modified LAS–X, Particle Measurement  
491 Systems, Boulder, Colorado) operated at 150°C and then at 300°C to remove volatile species. OPC  
492 was calibrated with a refractive index of 1.588 up to 2  $\mu\text{m}$  and 1.54 above that size, however dust  
493 absorption or asphericity were not accounted for and data are reported as optical diameter. A  
494 synthesis of dust size distribution defined a “reference dust” was calculated between surface and 6  
495 km height merging observations. The contribution of black carbon was subtracted from the  
496 ensemble of field sizes. The time of transport is not defined in the paper and we classified this dataset  
497 as MRT. In our treatment, and specifically for LEV2a data treatment, we assume that the optical to  
498 geometrical conversion is the same that the one estimated for the PCASP–100 as reported in  
499 Formenti et al. (2021). As a matter of fact the physical properties of the LAS–X (operating wavelength  
500 of 630 nm and opening angle of 35 to 120°) are very similar to the PCASP one. We report the size for  
501 the reference dust case as dN/dlogD as in their Figure 5c. Data are digitalized from the original  
502 publication.

- 503 ▪ **(Fratini et al., 2007): OPC, ground-based, geometrical diameter.** These authors used eddy covariance  
504 to measure the size-resolved flux of dust emitted over a sandy soil in the Gobi desert in Inner  
505 Mongolia, China. They measured the dust particle concentration by means an optical particle  
506 counter (OPC, CLIMET CI 3100), which sized particles within an equivalent aerodynamic diameter  
507 range of 0.35–9.5  $\mu\text{m}$ . The optical diameter was converted into an aerodynamic diameter following  
508 the formula  $D_{\text{aerod}} = D_{\text{opt}} (\rho_{\text{dust}})^{0.5} \cdot f(D_{\text{opt}}, m)$ , where the  $f(D_{\text{opt}}, m)$  function was estimated to be around  
509 0.85 as calculated assuming a refractive index of 1.53–0i and a soil particles density of 2.5  $\text{g cm}^{-3}$ . It  
510 resulted that the  $D_{\text{aerod}} = 1.35 \cdot D_{\text{opt}}$ . These measurements converted in aerodynamic diameter were  
511 then further corrected to geometric diameter by applying Equation (2) assuming a dust density of  
512  $2.5 \pm 0.2 \text{ g cm}^{-3}$  and a dynamic shape factor of  $1.4 \pm 0.1$  in (Kok et al., 2017). In this study we take  
513 data as reported in Kok et al. (2017) work and corresponding to the average of the three datasets  
514 shown in their Figure 10. Note that the Fratini et al. data  $> \sim 5 \mu\text{m}$  in diameter are unreliable because  
515 of the cutoff of the inlet system (Fratini personal communication as reported in Kok et al., 2017). In  
516 our treatment, and specifically for LEV2b conversion, we treat the Fratini dataset as aerodynamic  
517 diameter data following the approach of the original paper and the Kok et al. further analysis.  
518 Original data are fluxes as  $\text{dN cm}^{-2} \text{ s}^{-1}$  or  $\mu\text{g cm}^{-2} \text{ s}^{-1}$ . We took the treated data from Kok et al. (2017)  
519 as the average and standard deviation of the three cases in their Figure 10. Data were obtained from  
520 J. Kok (personal communication).
- 521 ▪ **(Kobayashi et al., 2007): Coulter multisizer, ground-based, geometrical diameter.** Aerosol sampling  
522 was conducted at four sites in Japan at Nagasaki (32°45N, 129°52E), Okayama (34°39N, 133°54E),  
523 Kofu (35°39N, 138°34E), and Tokyo (35°41N, 139°45E) in the period spring 2003 to spring 2004 and  
524 size distribution was measured with a Coulter multisizer providing the number concentration of  
525 water-insoluble aerosol particles in the diameter range of 0.4–12  $\mu\text{m}$ . Springtime was chosen as the  
526 time of the year when the Asian dust phenomena typically occur. The size distributions retrieved for  
527 the same Asian dust air mass varied at each sampling site and the volume mode diameter ranged  
528 from 1.4 to 2.2  $\mu\text{m}$ , reducing when going from west to east. The volume mode diameter was lower  
529 than identified in other Asian outflows, an observation explained by the possible internal mixing of  
530 Asian dust with other components and/or due to the breaking/dispersion of particles aggregates by  
531 ultrasonic shaking during extraction. The experimental protocol, improved for sampling in 2004,  
532 resulted in a larger dust mode in the range of 1–10  $\mu\text{m}$ . Data for this improved configuration were  
533 reported by these authors for two dust events measured at Kofu in March – April 2004. The  
534 measured mode diameters obtained by fitting with multi lognormal functions the data were 2.6–3.1  
535 and 4.3–5.6  $\mu\text{m}$  in these 2 Asian dust events. Data for the Kofu event are considered in the present  
536 analysis. The time of transport is not defined in the paper and we classified this dataset as MRT.  
537 Original data are expressed as  $\text{dV}/\text{dlnD}$  up to 10  $\mu\text{m}$  from their Figure 7. We consider here the  
538 average and standard deviation of data for two separate events (E2 to E4, identified as E1 – episode1,  
539 and E5 to E8, identified as E2 – episode2) corresponding to the two identified Asian dust episodes.  
540 Data were recalculated from the lognormal parameters shown in the original publication.
- 541 ▪ **(Otto et al., 2007): DMA + OPC (PCASP, FSSP-300), airborne, optical diameter.** These authors report  
542 on aerosol measurements acquired during the Aerosol Characterisation Experiment (ACE-2) flights  
543 on 8<sup>th</sup> of July 1997 about 50–200 km off the coast of Northern Africa close to Canary Islands. The  
544 aerosol size distributions was measured by five instruments, including Condensation Particle Counter  
545 (CPC), Differential Mobility Analyser (DMA), and PCASP and FSSP OPCs, and the data treatment  
546 followed the one described in (de Reus et al., 2000). During the flight a dust layer extending from 2.7  
547 to 5.8 km altitude was measured. Vertical-resolved size distribution data averaged over 100 m height  
548 were reported by the author in their Figure 3. Original data are expressed as  $\text{dN}/\text{dlogD}$  up to 31  $\mu\text{m}$   
549 form their Figure 3, we consider data at three specific levels (2700 m, 4000 m, 5500 m) where the  
550 dust layer was identified. Data are digitalized from the original publication.
- 551 ▪ **(Chou et al., 2008): microscopy, airborne, projected-area diameter.** Airborne aerosol measurements  
552 were performed during the AMMA / DABEX campaign between 13 January and 3 February 2006 on

553 board of the UK Bae-146 research aircraft. Flights explored the Western Africa and Sahel regions.  
554 The aerosol size distribution was retrieved for dust samples collected during 4 flights between 21  
555 and 30 January 2006 and corresponded to straight-levelled runs portions of the flight. The size  
556 distribution of dust particles was estimated by combining aerosol counting from the analysis of SEM  
557 (17 size classes ranging from 0.25 to 10  $\mu\text{m}$ ) and TEM (19 size classes ranging from 0.01 to 7  $\mu\text{m}$ )  
558 microscopy images. The retrieved size from microscopy analysis was in good agreement, and  
559 particularly below 0.5  $\mu\text{m}$  diameter, with observations obtained from a wing-mounted OPC as  
560 reported in (Osborne et al., 2008). For one of the four analyzed samples (B165N7) the authors  
561 identified the presence of anthropogenic particles as evidenced in microscopy images. We consider  
562 in this study the average and standard deviation of the size distribution for the four dust cases  
563 reported by Chou et al. in their Figure 6. Original data are reported as  $dN/d\log D$  in their Figure 6 as  
564 the combination of TEM (0.05 to 0.5  $\mu\text{m}$ ) and SEM (0.5 to 10  $\mu\text{m}$ ). Data were obtained from P.  
565 Formenti (personal communication).

566 ▪ **(McConnell et al., 2008): OPCs, airborne, optical diameter.** Measurements of dust size distribution  
567 were performed during the DODO campaign based at Dakar, Senegal, off the coast of North Africa.  
568 The DODO project occurred on two phases: a first one between 7 and 16 February 2006 (DODO-1),  
569 and the second one between 22 and 28 August 2006 (DODO-2). During the airborne operations a  
570 combination of wing-mounted OPCs were used including a PCASP and a cloud droplet probe  
571 (CDP-100). Additionally, optical microscopy on bulk filters were used to measure dust size  
572 distribution up to diameter of 40  $\mu\text{m}$ . We consider two datasets in this study, separately for the  
573 DODO-1 and the DODO-2 observations as obtained from the combination of PCASP and CDP  
574 observations. In our treatment, and specifically for LEV2a and LEV2b conversion, we assume that the  
575 main OPC data are those from the CDP, therefore optical to geometrical diameter corrections are  
576 taken from calculations of Formenti et al. (2021) for this OPC model. Original data are reported as  
577  $dN/d\log R$  normalized to the total number concentration as obtained for DODO-1 (retrieved from  
578 Figure 8 in Osborne et al. (2008), identified as dataset McConnell-1) and as  $dV/d\ln R$  normalized at  
579 the value at  $R=1 \mu\text{m}$  for DODO-2, retrieved from Figure 7 in McConnell et al. (2008) (identified as  
580 dataset McConnell-2). Data are digitalized from the cited publications.

581 ▪ **(Osborne et al., 2008): OPC, airborne, optical diameter.** Aerosol measurements were performed  
582 during the AMMA/DABEX campaign on board of the UK Bae-146 research aircraft using two OPCs:  
583 a wing-mounted Passive Cavity Aerosol Spectrometer Probe 100-X (PCASP) measuring in the  
584 diameter range 0.1–3.0  $\mu\text{m}$  and a PCASP-X measuring in the range 0.1–10  $\mu\text{m}$  diameter mounted  
585 inside the aircraft cabin that uses a virtual impactor inlet to measure particles up to diameter of 10  
586  $\mu\text{m}$ . It is reported in the paper that the size measurement efficiency was 100% in all size diameters  
587 for the PCASP wing-mounted, but not for the PCASP-X. In their paper, Osborne et al. [2008] found  
588 that the PCASP-X consistently overcounts when compared to the wing PCASP, and this was  
589 associated to a problem with the sample flow. In order to extend the size range of measurements  
590 from the wing PCASP, these authors corrected the PCASP-X by rescaling it to match the PCASP data  
591 in the region of overlap. They analyzed in their paper the impact of refractive index and  
592 non-sphericity in the PCASP measurements but reported data as calibrated for PSL particles and  
593 spherical assumption. In our treatment for LEV2a and LEV2b conversion, we assume the PCASP  
594 optical to geometrical diameter corrections calculated from Formenti et al. (2021) and extrapolated  
595 into a larger diameter range in our study to apply to both PCASP and PCASP-X. We report here the  
596 mean aerosol size distribution from the DABEX “pure” dust cases from the northeast of Niamey  
597 across the accumulation and coarse modes as shown in their Figure 8 and 9 and reported as  
598  $dN/d\log R$  normalized to the total number of particles. Data are digitalized from their Figure 9.

599 ▪ **(Rajot et al., 2008): OPC, ground-based, optical diameter.** Data from Banizoumbou (Niger) during the  
600 AMMA campaign in 2006 were used to derive statistics of dust size distribution under different  
601 conditions. Size data were obtained from optical particle counter (OPC, Grimm 1.108) measurements  
602 and were published as not corrected for the refractive index of dust. The OPC was installed behind

603 an Isokinetic Particle Collector inlet having a passing efficiency of about 50% at 40 $\mu$ m particle  
604 diameter. The used OPC measured up to  $\sim$ 30 $\mu$ m, but the authors discuss the possible presence of  
605 an additional coarser mode not detected by the used OPC. Data from their Figure 17 for local erosion  
606 events, labelled as L in their Figure, and for dust advected from distant sources, labelled as D in their  
607 Figure are considered in the present study as representative of SOURCE and MRT class events.  
608 Original data are dM/dlogD normalized by total mass. The average and standard deviation of the  
609 ensemble of D and L cases is considered in the present analysis. Data were obtained from J. L. Rajot  
610 (personal communication).

611 ▪ **(Reid et al., 2008): APS, ground-based, aerodynamic diameter.** As part of the United Arab Emirates  
612 Unified Aerosol Experiment (UAE2), the size distribution and chemistry of dust particles were  
613 measured for the months of August and September 2004 at an Arabian Gulf coastal site impacted by  
614 dust from several sources within southwest Asia. A TSI aerodynamic particle sizer model 3321 was  
615 used in the campaign. The APS sampled air from a common inlet through a heated (RH < 35%) line.  
616 The primary surface site utilized for the study was the Mobile Atmosphere Aerosol and Radiation  
617 Characterization Laboratory (MAARCO), located 50 km north of Abu Dhabi, UAE. The site, which was  
618 away from city plumes, mostly sampled air masses representative of the Arabian Gulf and the interior  
619 desert. Continuous coarse mode size distributions were measured during the campaign. The authors  
620 report data divided as Groups A and B in their Figure 2d, which reflect the two extremes in size for  
621 dust observations. Group A, with the smallest volume modal diameter (3.3  $\mu$ m), consisted of daily  
622 samples from 13 and 14 August and 23 September. Conversely, for the largest sized particles in group  
623 B (11, 12, 15, 30, and 31 August; 1, 12, 15, 16, 25, and 26 September) the 6  $\mu$ m volume mode was  
624 reported to be dominant compared to the 3  $\mu$ m mode. Original data are reported as dV/dlnD as  
625 aerodynamic diameter. Data are digitalized from their Figure 2d.

626 ▪ **(Sow et al., 2009): OPC, ground-based, optical diameter.** In their study Sow et al. used two optical  
627 particle counters (OPC, Grimm 1.108) at heights of 2.1 and 6.5 m to measure the size-resolved  
628 vertical flux of dust aerosols larger than 0.3  $\mu$ m in diameter. They reported measurements acquired  
629 during three dust storm events in Niger and corresponding to an average wind friction speed  
630 between 0.4 and 0.6 m s<sup>-1</sup>. Size data obtained from optical particle counter measurements were  
631 published as not corrected for the refractive index of dust. Original data are fluxes as dN m<sup>-2</sup> s<sup>-1</sup>. In  
632 our analysis we consider the average and standard deviation of the three cases shown in their Figure  
633 9. Data are obtained from J. Kok (personal communication).

634 ▪ **(Wagner et al., 2009): OPC, airborne, geometrical diameter.** In situ measurements of dust size  
635 distribution were performed in May 2006 over Portugal as part of the Desert Aerosols over Portugal  
636 (DAPRO) project affiliated with the SAMUM experiment. Airborne observations were performed  
637 from the FALCON aircraft using the same instrumental configuration and data treatment as in  
638 Weinzierl et al. (2009), with an high spectral resolution lidar additionally installed on the aircraft.  
639 Measurements of the size distribution between 0.01 and 35  $\mu$ m diameter obtained at 2300 m and  
640 3245 m height over Évora on 27 May 2006 were presented in their Figure 9. Ground based  
641 measurements of the size distribution were additionally obtained at the ground with an APS but we  
642 only considered airborne data in the present analysis. Original data are as dN/dlogD at STP conditions  
643 as reported in Figure 9 in Wagner et al.. Size distribution data at the two different heights were  
644 averaged and used as a single dataset in the following analysis. Data were digitalised from the original  
645 paper, their Figure 9.

646 ▪ **(Weinzierl et al., 2009): OPC, airborne, geometrical diameter.** These authors reported on size  
647 distribution observations acquired during the SAMUM1 airborne campaign from the German Center  
648 for Aviation and Space Flight DLR Falcon flights over Morocco in May and June 2006. Size distribution  
649 measurements were obtained from a set of different OPCs both wing-mounted or inside the aircraft  
650 cabin sampling aerosols through an isokinetic inlet with a 50% passing efficiency at about 2.5  $\mu$ m in  
651 diameter at the ground and 1.5  $\mu$ m at 10 km. Size instrumentation included a wing-mounted  
652 FSSP-300 measuring particles with diameters between 0.3 and 30  $\mu$ m, three Condensation Particle

653 Counters (CPCs, heated with a thermal denuder at 250°C) and a Grimm OPC. The three CPCs  
654 measured non-volatile particles in nucleation, Aitken, and accumulation mode, respectively, while  
655 the Grimm OPC measured non-volatile size distribution below 2.5 µm. The visible refractive index  
656 used to correct OPC dust data was 1.551–0.0028i (from Petzold et al., 2009). Three dust events were  
657 observed on 16 to 22 May, 24 to 28 May, and 31 May to 5 June during the campaign. The dust age  
658 for the observations during SAMUM1 was identified to be between 0 and 2 days. In this study we  
659 collocate the average of size observations from this study as MRT class. Original data are provided as  
660 dN/dlogD in the Weinzierl et al (2009) paper and the 4-modes fitting parameters of the dust size  
661 distribution during SAMUM1 are provided in Weinzierl et al. (2011). We use here the median of the  
662 SAMUM1 data as recalculated from the lognormal parameter fitting in the Weinzierl et al. (2011)  
663 paper, their Table 5, within the diameter range 0.1 to 50 µm. The range of variability was estimated  
664 using the 3th and 97<sup>th</sup> percentile values from the logfitting curves.

665 ▪ **(Müller et al., 2010): SMPS+APS, ground-based, geometrical diameter.** Size distribution observations  
666 were performed during the RHaMBLe (Reactive Halogens in the Marine Boundary Layer) campaign  
667 in May to June 2007 at Cape Verde. The particle size was measured by means of an SMPS between  
668 0.01 and 0.9 µm, in combination with an APS measuring between 0.6 and 10 µm. To combine the  
669 particle number size distributions of the SMPS and the APS, the aerodynamic particle diameters of  
670 the APS were converted to volume equivalent diameters, as described in the paper, however details  
671 of the assumptions are not provided. Therefore we consider that the conversion factor as in Eq. (2)  
672 is 1.0 in the present analysis. The size observations were combined in the SMPS–APS overlap  
673 diameters (0.7–0.9 µm). The inlet of the measurement system was installed 4m above the ground  
674 level on the top of a measurement container used during the campaign. Size distribution for 15 May  
675 2007 was reported and correspond to a dust-dominated case of aerosols transported from Western  
676 Africa. In our treatment we assume the APS to be the main instrument of reference for LEV2a and  
677 LEV2b corrections in both datasets. Original data are reported as number distribution in their Figure  
678 8. Data are digitalized from the original paper, their Figure 8.

679 ▪ **(Chen et al., 2011): USHAS + APS, airborne, geometrical diameter.** Aerosol size distributions during  
680 the NAMMA campaign in the Tropical Atlantic for the 0.07 to 1 µm diameter range were measured  
681 with an Ultra-High Sensitivity Aerosol Spectrometer (UHSAS) manufactured by Droplet  
682 Measurement Technologies and by means of a TSI model 3321 Aerodynamic Particle Sizer (APS) in  
683 the 0.7 to 5 µm aerodynamic diameter range. Data corresponds to dry conditions that is relative  
684 humidity (RH) less than 30%. The upper size limit of measurements indicates the inlet size cut. As  
685 discussed in the main paper, only UHSAS data up to 0.6 µm diameter were used due to instrument  
686 problems related to a reduced counting efficiency at the larger sizes during the NAMMA deployment.  
687 The UHSAS was calibrated before the campaign and also periodically during operations using latex  
688 spheres, and it was not operational for the second half of the NAMMA campaign. The APS instrument  
689 was calibrated with both latex and silicon spheres; dust particle aerodynamic diameters were  
690 converted to geometric diameters using the dynamic shape factor of 1.6 and particle mass density  
691 of 2.6 g cm<sup>-3</sup>. In our treatment we assume the APS to be the main instrument of reference for LEV2a  
692 and LEV2b corrections in both datasets. Original data are reported both as dN/dlogD and dV/dlogD  
693 in their Figure 5 and error bars in the Figure represent one standard deviation estimated during the  
694 dust layer sampling period. Data are digitalized from the original paper, their Figure 5.

695 ▪ **(Formenti et al., 2011): OPC, airborne, geometrical diameter.** Airborne data of dust size distribution  
696 over Niger were acquired from aircraft observations during the AMMA campaign in June–July 2006.  
697 Size distribution were obtained from an OPC (Grimm 1.108) whose measurements were corrected  
698 for the refractive index of dust by assuming a refractive index in the visible of 1.53–0.002i. The OPC  
699 was installed on an ATR-42 on the iso-axial and isokinetic AVIRAD inlet having a 50% passing  
700 efficiency at about 9 µm in diameter. The size distribution for different local erosion and Sharan  
701 transport events were reported in their Figure 10. In this paper we consider average data for V018  
702 and V028 corresponding to local erosion event sampled with the aircraft at about 700 m asl 1–2 days

703 after emission and the average of V021, V022, and V036 as representative of mid-range transport  
704 conditions for dust sampled at about 2500 m asl. Data in the original paper are reported as  $dv/d\log D$   
705 normalized to the total number concentration. Data are obtained from P. Formenti (personal  
706 communication).

707 ▪ **(Johnson and Osborne, 2011): OPCs, airborne, geometrical diameter.** Size distribution data for dust  
708 events over the western region of the Sahara desert were obtained during the GERBILS campaign  
709 from the UK Facility for Airborne Atmospheric Measurements (FAAM) BAe-146 aircraft. Vertical  
710 profiles acquired during ten flights showed dust layers at varying altitudes extending up to 6.5 km in  
711 the troposphere. Aerosol size distributions were measured in situ by two wing-mounted OPCs  
712 including a Passive Cavity Aerosol Spectrometer Probe (PCASP-100X) for the accumulation mode in  
713 the nominal diameter range 0.1–3.0  $\mu\text{m}$  and a Small Ice Detector (SID-2) for coarse mode particles  
714 in the 2–60  $\mu\text{m}$  nominal diameter range. The PCASP optical diameter was converted into a  
715 geometrical diameter by using Mie theory and a refractive index of  $1.53 + 0.0015i$ . The SID-2  
716 observations were corrected for the combined effects of particle shape and refractive index by  
717 applying T-matrix calculations. In our treatment we further correct these data, which already partly  
718 account for particle non sphericity, to a LEV2b dataset using an average ASR function as described in  
719 Text S4. The average of the dust distribution observations for the campaign was reported in their  
720 Figure 3 and modelled as a four modes lognormal size distribution. Original data are  $dN/d\log D$ . Data  
721 are recalculated from the logfit parameters corresponding to the dust average size in Table 2.

722 ▪ **(Kandler et al., 2011): DMS+APS+microscopy, ground-based, projected-area diameter.**  
723 Measurements of the size distribution of aged dust were performed as part of the SAMUM-2  
724 campaign in 2008, following the fresh dust characterization exercise during the SAMUM-1 campaign  
725 in 2006 (Weinzierl et al., 2009). Kandler et al. (2011) used the similar instrumentation as at the  
726 ground site of Tinfou during SAMUM-1 to measure dust size distribution at a ground station on Praia,  
727 Cape Verde in winter 2008. The aerosol size distributions in the submicron range were measured by  
728 a combination of a DMPS (mobility size range of 26–800 nm) and an APS (model 3321, TSI Inc., St.  
729 Paul, USA; aerodynamic size range of 570 nm to 10  $\mu\text{m}$ ). For the APS only data for particles smaller  
730 than 5  $\mu\text{m}$  were used. The aerodynamic diameters were converted into volume equivalent diameters  
731 using an effective density of 2 g  $\text{cm}^{-3}$ , as documented in Schladitz et al. (2011). Particles in the size  
732 range of 4–500  $\mu\text{m}$  were collected by a single-stage impactor and analysed by microscopy. The setup  
733 allowed to reduce the the size error to 3% for particles larger than 15  $\mu\text{m}$ , and approximately 0.5  $\mu\text{m}$   
734 for smaller ones. The same corrections, procedure and image analysis as described by Kandler et al.  
735 (2009) were applied in Kandler et al. (2011). In our treatment we assume the microscopy to be the  
736 main reference technique for LEV2a and LEV2b correction data. Original size distributions data from  
737 three dust phases of the SAMUM2 campaign characterized by transport from the eastern  
738 Mali/western Niger area (DU2 and DU3) and southern Mauritania (shorter distance, DU1) are  
739 reported in their Figure 6 as  $dN/d\log D$  and  $dV/d\log D$ . They also report the volume size distributions  
740 for the averages of dust periods on Cape Verde and this volume distribution is used in the present  
741 study. Data are digitalized from the original paper, their Figure 6.

742 ▪ **(Shao et al., 2011): OPC, ground-based, geometrical diameter.** These authors reported  
743 measurements of the vertical dust flux as observed for a strong erosion event on a flat agricultural  
744 field in Australia during the Japanese Australian Dust Experiment (JADE) in 2006. An OPC (YGK Corp.  
745 ADS-03-8CH) was used to measure the particle concentration in the 0.3–8.4  $\mu\text{m}$  geometric diameter  
746 size range at 1.0, 2.0, and 3.5 m heights. Optical to geometrical diameter conversion was performed  
747 assuming a CRI of  $1.5-0.001i$  and modeling dust as tri axis oval shape (Huang et al., 2021  
748 supplementary information). These measurements were combined with wind speed observations to  
749 calculate the vertical dust flux as a function of friction velocity. The authors questioned the reliability  
750 of the 0.3 – 0.6  $\mu\text{m}$  size bin, as discussed in Kok et al. 2017. In our treatment we further correct these  
751 data, which already partly account for particle non sphericity, to a LEV2b dataset using an average  
752 ASR function as described in Text S4. Original data are fluxes as  $dN \text{ m}^{-2} \text{ s}^{-1}$ . We took the treated data

753 from Kok et al. (2017) (average and standard deviation of the three cases in Fig. 12 from Shao et al.  
754 (2011)). Data are obtained from J. Kok (personal communication).

755 ▪ **(Weinzierl et al., 2011): OPCs, airborne, geometrical diameter.** These authors report airborne  
756 observations from flights around the Cape Verde area during the SAMUM-2 campaign in 2008.  
757 Different OPCs, both wing-mounted on the DLR Falcon aircraft or inside the cabin, were used. The  
758 wing mounted had a 50% passing efficiency of 30  $\mu\text{m}$ , whereas the cabin OPC sampled aerosols  
759 through an isokinetic inlet having a 50% passing efficiency at about 2.5  $\mu\text{m}$  in diameter at the ground  
760 and 1.5  $\mu\text{m}$  at 10 km. The visible refractive index used to correct OPC dust data was  
761 1.55-0.003/0.004i as reported in their Table 3. Original data are reported as  $dN/d\log D$ . We use here  
762 the 4-modes fitting parameters as reported in the Weinzierl et al. (2011) paper, their Table 5, for  
763 the median of the SAMUM-2 data calculated within the diameter range 0.1 to 30  $\mu\text{m}$  (upper limit of  
764 the inlet). The range of variability is estimated using the 3th and 97<sup>th</sup> percentile values from the  
765 logfitting curves

766 ▪ **(Jung et al., 2013): OPC, airborne, optical diameter.** Airborne in situ measurements of dust size  
767 distribution was performed onboard Center for Interdisciplinary Remotely Piloted Aircraft Studies  
768 (CIRPAS) Twin Otter in the framework of the Barbados Aerosol Cloud Experiment (BACEX) in  
769 March-April 2010. Size distribution was measured by means of a PCASP OPC in the range of 0.1-2.5  
770  $\mu\text{m}$ . Two dust episode measurements were taken on the 1st of April within the Sahara air layer (SAL)  
771 at 2306 m, and on the 2nd of April in the SAL at 1930 m, showing very similar size distributions. We  
772 consider here the average of the datasets. Original data are shown as both number and volume  
773 distributions. Data are digitalized from the original paper, their Figure 14 c and d.

774 ▪ **(Ryder et al., 2013a; 2013b): OPC + OAP, airborne, geometrical diameter.** These two papers  
775 synthesize measurements of the dust size distribution obtained during the FENNEC campaign in June  
776 2011 over the western African desert, covering Mauritania, Mali and Canary islands, based on  
777 observations from the UK's Bae-146-301 Research Aircraft. Research flights included a total of 42  
778 profiles acquired in an altitude range between 100 m up to around 8 km, but with most of the  
779 measurements corresponding to levels below 2-3 km. Several instruments were combined to  
780 measure the dust size distribution over a large size range, including wing-mounted PCASP 100X, CDP  
781 and CAS models OPCs, and CIP cloud probe. The measurement setup during FENNEC was in particular  
782 conceived to increase the confidence in the coarse mode size distribution measurements, in  
783 particular the coarse fraction up to 40 to 100  $\mu\text{m}$  diameter, covered by different instruments  
784 simultaneously. Instrumental calibration, drift and for a refractive index of dust were accounted for  
785 in the analysis. The OPC dust data were corrected using Mie theory and assuming a real refractive  
786 index of 1.53 and an imaginary refractive index between 0.001 and 0.003 in the visible range. Data  
787 for three categories namely fresh dust, representing dust uplifted within 12 h prior observations,  
788 aged dust, for dust uplifted within 12 to 70 hours before observations, and SAL aerosols,  
789 corresponding to plumes with a mean age of 87 hours, are reported in the Ryder et al. work. In our  
790 treatment we assume the OPC data to be the main reference technique for LEV2b correction data.  
791 Original data are reported as volume size distribution. Averaged data for the three categories are  
792 obtained from C. Ryder (personal communication).

793 ▪ **(Rosenberg et al., 2014): OPC + OAP, airborne, geometrical diameter.** Rosenberg et al. report  
794 measurements of the size-resolved aerosol fluxes up to 300  $\mu\text{m}$  diameter as retrieved by the  
795 combination of two OPCs and an OAP using eddy covariance technique. The measurements were  
796 acquired during the FENNEC airborne campaign as described in (Ryder et al., 2013b) and refer to  
797 altitudes ranging between  $\sim 100 - 1000$  m asl. Data were categorized as four different regions and at  
798 three different ranges of the vertical turbulent kinetic energy. The calibrations and the optical to  
799 geometrical diameter for OPC instruments is based on (Rosenberg et al., 2012) and assumes a  
800 refractive index of 1.53-0.001i for dust in the visible range. In our treatment, as for Ryder et al.  
801 (2013a; 2013b) we assume the OPC data to be the main reference technique for LEV2b correction  
802 data. Original data are mass and number fluxes as  $dN\text{ m}^{-2}\text{ s}^{-1}$  or  $dM\text{ m}^{-2}\text{ s}^{-1}$ . We took the treated

803 data from Kok (average and standard deviation of the cases in Fig. 5 for data between 0.5 and 20  
804  $\mu\text{m}$ ) to which we add the average data above 20  $\mu\text{m}$  as digitalized from the original paper, their  
805 Figure 5.

806 ▪ **(Meloni et al., 2015).** *OPC, airborne, optical diameter.* The measurements were taken in spring 2008  
807 over the sea surface at the island of Lampedusa during the Ground-based and Airborne  
808 Measurements of Aerosol Radiative Forcing (GAMARF) campaign. Aircraft observations of the dust  
809 size distribution during an intense outbreak episode on the 3rd of May 2008 were obtained for dust  
810 originating in Morocco. A model 1.108 Grimm (OPC) measured the number of particles in a nominal  
811 diameter range covering the range 0.3 to 20  $\mu\text{m}$  in 15 size channels. The size distribution from the  
812 Grimm measurements was integrated over the 1000 to 2000 m altitude where dust was present,  
813 and fitted with a 3-mode lognormal function. We use the 3 modes function to reproduce the dust  
814 distribution. Original data are normalized volume size distributions as shown in the original paper in  
815 their Figure S1 panel b. Data are obtained from D. Meloni (personal communication).

816 ▪ **(Denjean et al., 2016a).** *SMPS+OPC, airborne, geometrical diameter.* The size distribution of dust  
817 aerosols was measured during the Dust-ATTACK field campaign that took place between 20 June  
818 and 13 July 2012 at the Cape San Juan Puerto Rico Aerosol Observatory. Instruments were installed  
819 behind a standard NOAA/ESRL/GMD aerosol inlet and measurements were performed at relative  
820 humidity below <40%. The particle number size distribution was measured by a combination of a  
821 SMPS, working in the 11.8–593.5 nm mobility diameter range, and a GRIMM 1.109 OPC, measuring  
822 within 0.25–32  $\mu\text{m}$  equivalent optical diameter range. The SMPS mobility diameter was converted  
823 into a geometric diameter assuming a dry dynamic shape factor of  $1.2 \pm 0.09$ , discussed in the paper  
824 to be a good approximation for randomly oriented elongated particles. The OPC optical to geometric  
825 diameter conversion was performed assuming a refractive index of  $1.53 - 0.002i$  and Mie theory for  
826 homogeneous spherical particles. Several dust events were recorded at Puerto Rico during  
827 DUST-ATTACK, with PM10 concentrations increases from 20 to 70  $\mu\text{g m}^{-3}$  during the events. Main  
828 source regions were identified to localize in the Western Sahara, Mauritania, Algeria, Niger, and Mali.  
829 The volume size distributions ( $dV/d\log D$ ) from SMPS and GRIMM, normalized to the total volume,  
830 for the five dust events observed during the field campaign are reported in their Figure 8. The most  
831 dust-dominated event occurred on the 3rd of July, classified as E3 (episode 3), and considered here  
832 as representative dust size distribution data for this campaign. The average and standard deviation  
833 for the size distribution data for E3 are used here. In our treatment we assume the OPC data to be  
834 the main reference technique for LEV2b correction data. Original data are normalized volume size  
835 distributions as shown in the original paper in their Figure 8. Data were obtained from C. Denjean  
836 (personal communication).

837 ▪ **(Denjean et al., 2016b).** *SMPS+OPCs, airborne, geometrical diameter.* The size distribution of dust  
838 aerosols transported into the Mediterranean basin was measured during the ChArMEx/ADRIMED  
839 (the Chemistry-Aerosol Mediterranean Experiment/Aerosol Direct Radiative Impact on the regional  
840 climate in the MEDiterranean region) field campaign in June-July 2013 on board of the aircraft  
841 ATR-42. The number size distribution in the submicron range was measured with an in-cabin SMPS  
842 combined with a wing-mounted UHSAS OPC; the supermicron size was measured by two different  
843 OPCs : a wing-mounted FSSP-300 and a GRIMM 1.129. The electrical mobility diameters by the  
844 SMPS are converted into geometrical diameters assuming a dynamic shape factor of 1, therefore  
845 assuming particle sphericity. The OPCs optical diameters were converted into geometrical diameters  
846 by assuming a refractive index of  $1.53 - 0.004i$  and homogeneous spherical particles. During  
847 ADRIMED, systematic differences in the size distributions measured by the FSSP-300 and the GRIMM  
848 were observed around 2  $\mu\text{m}$ . Data between 2–10  $\mu\text{m}$  and 1.5–2  $\mu\text{m}$  diameter from the FSSP-300  
849 and the GRIMM respectively were not considered in the original paper analysis. The GRIMM OPC  
850 was behind the AVIRAD inlet, having a cut-off diameter value of 12  $\mu\text{m}$  as optical equivalent  
851 diameter, while the SMPS was set up behind the Community Aerosol Inlet (CAI), having a cut-off at  
852 5  $\mu\text{m}$ . The USHAS and the FSSP were wing-mounted therefore not affected by inlet cut-off limits.



853 Different dust episodes were encountered during the ADRIMED campaign at altitudes between 1000  
854 and 5400 m, with dust originated between 1 and 5 days before in Tunisia, Morocco and Algeria. The  
855 average of all dust observations above 3000 m during the ADRIMED campaign, reported to be less  
856 contaminated by pollution than observations below this altitude, is considered here. The absolute  
857 variation between the maximum and the minimum of the average measured size distribution is  
858 assumed as the data uncertainty in the present analysis. In our treatment we assume the OPC data  
859 to be the main reference technique for LEV2b correction data. Original data are reported as  
860 normalized volume size distribution in their Figure 7b. Data were are digitalized from the original  
861 paper, their Figure 5.

862 ▪ **(Struckmeier et al., 2016).** APS, ground-based, aerodynamic diameter. The size distribution was  
863 measured at Rome during the DIAPASON campaigns. Measurements were performed with an APS  
864 providing aerosol sizing between 0.5 and 20  $\mu\text{m}$  aerodynamic diameter. Two DIAPASON field  
865 campaigns occurred in 2013 and 2014. Dust advection event lasting for several days was observed  
866 both years, one between 23 October and 1 November 2013, and 20 to 26 May 2014. The event in  
867 2014 was much more intense than the one in 2013 and it is the one considered here. In 2014 dust  
868 originate at 30–35°N between Morocco (Saharan Atlas) and Tunisia (Erg Oriental). Original data are  
869 mass size distributions. Data are digitalized from the original paper, their Figure 3.

870 ▪ **(Weinzierl et al., 2017).** OPCs, airborne, geometrical diameter. Airborne in situ aerosol size  
871 distribution measurements were obtained in the framework of the Saharan Aerosol Long-Range  
872 Transport and Aerosol-Cloud-Interaction Experiment (SALTRACE) in June 2013 with a Falcon  
873 research aircraft. A lagrangian-type study was performed during the campaign and consisted in  
874 sampling the same air mass first over Cabo Verde at the altitude of 2.6 km on 17 June 2013, and  
875 again over Barbados at 2.3 km on 22 June 2013 after its transport across the Atlantic Ocean. The  
876 aerosol total number distribution below 1  $\mu\text{m}$  was retrieved by combining measurements from three  
877 Condensation Particle Counters (CPCs), and a Grimm 1.129 OPC, all instruments installed behind an  
878 isokinetic inlet cutting particles at 2.5  $\mu\text{m}$  diameter. Three different wing-mounted OPCs (UHSAS-A,  
879 GRIMM, FSSP) covering the nominal size range 0.06–30  $\mu\text{m}$ , and a CAS-DPOL OPC measuring  
880 between 0.5 and 50  $\mu\text{m}$  were set up for coarse dust sizing. Measured size data were inverted with a  
881 consistent Bayesian inversion procedure following the procedure described by (Walser et al., 2017).  
882 The full size distribution obtained was parametrized with four lognormal distributions. Original data  
883 are number size distributions as shown in Figure 9 in their paper providing a synthesis of Cabo Verde  
884 and Barbados observations. Data are digitalized from the original paper, their Figure 9.

885 ▪ **(Moran Zuloaga et al., 2018)** OPC, ground-based data, optical diameter. Measurements were  
886 acquired in Brasil at the site of ATTO tower for the period 2014 to 2017 and contributed to the  
887 GoAmazon 2014/5 campaign. Size distribution was derived based on OPC measurements (OPS,  
888 model 3330, TSI Inc. Shoreview, MN, USA) operated continuously at the ATTO site since 30 January  
889 2014. The OPC was set at a resolution of 5 minutes and data covered a 38 months period for the  
890 analysis presented in the original paper. The OPC instrument allowed sizing aerosols between 0.3  
891 and 10  $\mu\text{m}$  in 16 bins. It was located in a container at the base of a triangular mast sampling ambient  
892 air from a 25 mm stainless steel sampling line with a total suspended matter (TSP) inlet located at 60  
893 m a.g.l., which corresponds to about 30 m above the canopy height. The sample air was dried to a  
894 relative humidity (RH) of about 40 %. The measured aerosol number size distributions were  
895 converted into surface and volume size distributions assuming that particles are spherical (shape  
896 factor of 1) and that their density is 1  $\text{g cm}^{-3}$ . We consider here the volume size distribution data  
897 they reported in their Figure 6 for the advected African dust corresponding to the long range  
898 transport episodes identified (median curve as reported in their Figure 6d). In our treatment, and  
899 specifically for LEV2a data treatment, we assume that the optical to geometrical conversion is the  
900 same that the one estimated for the GRIMM 1.109 as reported in Formenti et al. (2024). As a matter  
901 of fact the physical properties of the OPS considered in this paper (operating wavelength of 660 nm  
902 and opening angle of 30 to 150°) are very similar to the GRIMM one. Original data are volume size

903 distributions as shown in Figure 6d in their paper. Data are taken from Table S6 in the supplement  
904 of the original paper.

905 ▪ **(Renard et al., 2018).** OPC, airborne, optical diameter. Balloon borne observations of the dust size  
906 distribution were obtained during the ChArMEx intensive campaign in June–July 2013 in the western  
907 part of the Mediterranean basin. Measurements were performed with the LOAC OPC installed and  
908 flying on drifting boundary layer pressurised balloons (BLPBs). Different flights were performed with  
909 the LOAC during African dust plume events of the ChArMEx summer 2013 campaign. One example  
910 of measurement of the particle volume size distribution within the desert dust plume from the BLPB  
911 flight of 19 June 2013 at an altitude of 3.3 km is reported in their Figure 15. In our treatment, and  
912 specifically for LEV2b conversion, the data are left unchanged and this because of the nominal  
913 technical properties of the LOAC, measuring particle scattering in the 12° forward direction discussed  
914 by the authors to be mostly insensitive to refractive index calibration. Original data are volume size  
915 distributions as shown in Figure 15(a) in their paper. Data are digitalized from the original paper,  
916 their Figure 15.

917 ▪ **(Ryder et al., 2018).** OPC + CIP, airborne, geometrical diameter. These authors report airborne in situ  
918 measurements of the dust size distribution as obtained in August, 2015 close to Cape Verde during  
919 the AERosol Properties –Dust (AER–D) campaign based on UK’s Bae–146–301 Research Aircraft  
920 operations. The configuration was similar to the one during Fennec 2011 campaign, but in addition  
921 the AER–D campaign used cloud imaging probes (CIP15 and 2DS) for size distributions at diameters  
922 larger than 10 µm. Wing–mounted OPCs (PCASP and CDP) and shadow probes were combined to  
923 measure dust sizes between 0.1 and 100 µm diameter. The OPCs optical to geometrical diameter  
924 conversion was performed assuming Mie theory and a dust refractive index of 1.53–0.001i. The  
925 paper presents size distributions from 31 profiles and 19 in situ aerosol horizontal sampling runs. Of  
926 these, 14 horizontal runs sampled dust in the SAL at altitudes between 1.8 and 4.1 km. The age of  
927 sampled dust varied between 1 and 5 days. The AER–D mean logfit size distributions from the SAL  
928 observations reported in their Figure 6 are considered here. Original data are mean, min and max  
929 volume size distributions as shown in the original paper in their Figure 6. Data were recalculated  
930 from the lognormal fitting parameters in their Table 5 (from the corrigendum version).

931 ▪ **(Huang et al., 2019).** OPC, ground–based, geometrical diameter. In situ field measurements of the  
932 dust size distribution at emission were acquired from a coastal sand sheet at Oceano Dunes in  
933 California from 15 May to 7 June 2015. They used six OPCs (the 212 ambient particulate profiler,  
934 manufactured by Met One Instruments, Inc.), four of which were mounted on a tower at four  
935 different heights within 0.74–6.44 m above the surface. Each OPC measured size–resolved aerosol  
936 concentrations using seven size bins with optical equivalent diameters within the range 0.49–10 µm.  
937 Of the seven size bins, only the smallest six bins with nominal diameters ranging from 0.49 to 7 µm  
938 were used, while the seventh one was removed because of reduced sampling efficiency, in particular  
939 under strong winds. The OPCs optical diameters were converted into geometric diameter using Mie  
940 calculation and a CRI of 1.53–0.003i. Normalized volume particle size distribution of dust at emission  
941 as reported in their Figure 3 and is considered in this study. Original data are volume size  
942 distributions. Data are digitalized from the original paper, their Figure 3.

943 ▪ **(Khalfallah et al., 2020).** OPC, ground–based, geometrical diameter. Size distribution for dust erosion  
944 events were reported for observations performed during the WIND-O-V's (WIND erOsion in presence  
945 of sparse Vegetation) experiment in March to May 2017 in Tunisia, Northern Africa. Size number  
946 fluxes were measured at 2 and 4 m above ground level by means of two OPCs (PALAS Welas). Each  
947 OPC was equipped with an omnidirectional total suspended particles (TSP) sampling head for which  
948 the collection efficiency varied with wind speed and ranged from 79% at 0.56 m/s to 99% at 2.2 m/s,  
949 and 102% at 6.7 m/s for a mass median diameter of 15 µm. Because the range of wind velocity  
950 measured during the emission periods was >5 m/s at about 2 m, it is expected that no significant loss  
951 of coarse particles occurred. The optical to geometrical diameter conversion was performed by Mie  
952 theory assuming a refractive index of 1.43–0i, considered a value representative for silica. The OPCs

953 measured the size distributions of the vertical number dust flux for 8 dust emission events lasting  
954 for 5 to 9 hours each. Original data are reported as the average of the size distribution over the  
955 duration of each event in their Figure 5 as  $\text{dN cm}^{-2} \text{s}^{-1}$ . The average and standard deviation of the  
956 size obtained for the eight events is considered in the present study. Data are digitalized from the  
957 original paper, their Figure 5.

958 ▪ **(González-Flórez et al., 2023).** **OPC, ground-based, geometrical diameter.** Size distribution for dust  
959 erosion events were reported for observations performed at the ground during a field campaign in  
960 the Moroccan Sahara in September 2019. The campaign was in the context of the FRontiers in dust  
961 minerAloGical coMposition and its Effects upoN climaTe (FRAGMENT) project. Size number fluxes  
962 were measured at 1.8 and 3.5 m above ground level by means of two OPCs (Fidas 200S, Palas GmbH)  
963 sampling from a Sigma-2 head (Palas GmbH). The sampling efficiency of the sampling head was not  
964 measured, but the authors indicate that it is insensitive to wind speed up to  $6\text{ms}^{-1}$  in the PM10 range  
965 by previous studies. The used OPC sizes particles in 63 size bins (equally-spaced in logarithmic scale)  
966 in a nominal diameter range of 0.2 to  $19.1 \mu\text{m}$ . Data from the first three bins of the OPCs ( $< 0.25 \mu\text{m}$ )  
967 were discarded because reported to show unrealistic behaviour. The measured number particle  
968 concentrations were averaged over 15 min and classified over different intervals of friction velocity.  
969 The optical to geometrical diameter conversion of the OPCs diameters was performed assuming  
970 ellipsoidal dust particles based on a database of shape-resolved single scattering properties as in  
971 Huang et al. (2021). For initializing the calculations an aspect ratio (AR) of 1.46 is assumed, at the  
972 median of the measurements during the campaign based on microscopy analysis, while the height-  
973 to-width ratio (HWR) is set at  $0.45 \mu\text{m}$ . A refractive index of  $1.49-0.0015i$  is assumed for Moroccan  
974 dust. Emission size distribution data are reported in the paper as averages over different classes of  
975 friction velocity and for well-developed erosion conditions during regular events and for two haboob  
976 events. In this study we consider the size distribution for regular events corresponding to friction  
977 velocity range of  $0.30$  to  $0.35 \text{ m s}^{-1}$  (at the middle of their investigated range) as representative of  
978 the campaign data. To note that data from this study within the range  $11.25-17.83 \mu\text{m}$  are not taken  
979 into account for LEV2b mean calculations presented in Fig. 2 and 3 for the SOURCE category in the  
980 main as they strongly biased the mean size in this specific range. They are taken into account in the  
981 standard deviation calculation. Original data are reported as the average normalized emission flux  
982 size distribution for well-developed erosion conditions during regular events in their Figure 13 (panel  
983 e). The size obtained for the average friction velocity range of  $0.30-0.35 \text{ m s}^{-1}$  is considered in the  
984 present study. Data are digitalized from the original paper, their Figure 13.

985  
986

987 **Supplementary references**

- 988 d'Almeida, G. A.: On the variability of desert aerosol radiative characteristics, 92, 3017–3026,  
989 <https://doi.org/10.1029/JD092iD03p03017>, 1987.
- 990 d'Almeida, G. A. and Schütz, L.: Number, Mass and Volume Distributions of Mineral Aerosol and Soils of the Sahara,  
991 *J. Climate Appl. Meteor.*, 22, 233–243, [https://doi.org/10.1175/1520-0450\(1983\)022<0233:NMAVDO>2.0.CO;2](https://doi.org/10.1175/1520-0450(1983)022<0233:NMAVDO>2.0.CO;2),  
992 1983.
- 993 Basart, S., Pérez, C., Cuevas, E., Baldasano, J. M., and Gobbi, G. P.: Aerosol characterization in Northern Africa,  
994 Northeastern Atlantic, Mediterranean Basin and Middle East from direct-sun AERONET observations, *Atmos.*  
995 *Chem. Phys.*, 9, 8265–8282, <https://doi.org/10.5194/acp-9-8265-2009>, 2009.
- 996 Bates, T. S., Coffman, D. J., Covert, D. S., and Quinn, P. K.: Regional marine boundary layer aerosol size distributions  
997 in the Indian, Atlantic, and Pacific Oceans: A comparison of INDOEX measurements with ACE-1, ACE-2, and  
998 *Aerosols*99, 107, INX2 25-1-INX2 25-15, <https://doi.org/10.1029/2001JD001174>, 2002.
- 999 Chen, G., Ziemba, L. D., Chu, D. A., Thornhill, K. L., Schuster, G. L., Winstead, E. L., Diskin, G. S., Ferrare, R. A.,  
1000 Burton, S. P., Ismail, S., Kooi, S. A., Omar, A. H., Slusher, D. L., Kleb, M. M., Reid, J. S., Twohy, C. H., Zhang, H., and  
1001 Anderson, B. E.: Observations of Saharan dust microphysical and optical properties from the Eastern Atlantic  
1002 during NAMMA airborne field campaign, 11, 723–740, <https://doi.org/10.5194/acp-11-723-2011>, 2011.
- 1003 Chou, C., Formenti, P., Maille, M., Ausset, P., Helas, G., Harrison, M., and Osborne, S.: Size distribution, shape, and  
1004 composition of mineral dust aerosols collected during the African Monsoon Multidisciplinary Analysis Special  
1005 Observation Period 0: Dust and Biomass-Burning Experiment field campaign in Niger, January 2006, 113,  
1006 <https://doi.org/10.1029/2008JD009897>, 2008.
- 1007 Clarke, A. D., Shinozuka, Y., Kapustin, V. N., Howell, S., Huebert, B., Doherty, S., Anderson, T., Covert, D., Anderson,  
1008 J., Hua, X., Moore, K. G., McNaughton, C., Carmichael, G., and Weber, R.: Size distributions and mixtures of dust  
1009 and black carbon aerosol in Asian outflow: Physicochemistry and optical properties, 109,  
1010 <https://doi.org/10.1029/2003JD004378>, 2004.
- 1011 De Carlo, P.F., Jay G. Slowik, Douglas R. Worsnop, Paul Davidovits & Jose L. Jimenez (2004) Particle Morphology  
1012 and Density Characterization by Combined Mobility and Aerodynamic Diameter Measurements. Part 1: Theory,  
1013 *Aerosol Science and Technology*, 38:12, 1185–1205, DOI: 10.1080/027868290903907.
- 1014 Denjean, C., Formenti, P., Desboeufs, K., Chevaillier, S., Triquet, S., Maillé, M., Cazaunau, M., Laurent, B., Mayol-  
1015 Bracero, O. L., Vallejo, P., Quiñones, M., Gutierrez-Molina, I. E., Cassola, F., Prati, P., Andrews, E., and Ogren, J.:  
1016 Size distribution and optical properties of African mineral dust after intercontinental transport, 121, 7117–7138,  
1017 <https://doi.org/10.1002/2016JD024783>, 2016a.
- 1018 Denjean, C., Cassola, F., Mazzino, A., Triquet, S., Chevaillier, S., Grand, N., Bourriane, T., Momboisse, G., Sellegri,  
1019 K., Schwarzenbock, A., Freney, E., Mallet, M., and Formenti, P.: Size distribution and optical properties of mineral  
1020 dust aerosols transported in the western Mediterranean, 16, 1081–1104, [https://doi.org/10.5194/acp-16-1081-](https://doi.org/10.5194/acp-16-1081-2016)  
1021 2016, 2016b.
- 1022 Dubovik, O., and King, M. D.: A flexible inversion algorithm for retrieval of aerosol optical properties from Sun and  
1023 sky radiance measurements, *J. Geophys. Res.*, 105, 20673–20696, <https://doi.org/10.1029/2000JD900282>, 2000.
- 1024 Dubovik, O., Sinyuk, A., Lapyonok, T., Holben, B. N., Mishchenko, M., Yang, P., Eck, T. F., Volten, H., Muñoz, O.,  
1025 Veihelmann, B., van der Zande, W. J., Leon, J.-F., Sorokin, M., and Slutsker, I.: Application of spheroid models to  
1026 account for aerosol particle non sphericity in remote sensing of desert dust, *J. Geophys. Res.*, 111, D11208,  
1027 <https://doi.org/10.1029/2005JD006619>, 2006.
- 1028 Formenti, P., Andreae, M. O., Lange, L., Roberts, G., Cafmeyer, J., Rajta, I., Maenhaut, W., Holben, B. N., Artaxo, P.,  
1029 and Lelieveld, J.: Saharan dust in Brazil and Suriname during the Large-Scale Biosphere-Atmosphere Experiment  
1030 in Amazonia (LBA) – Cooperative LBA Regional Experiment (CLAIRE) in March 1998, 106, 14919–14934,  
1031 <https://doi.org/10.1029/2000JD900827>, 2001.
- 1032 Formenti, P., Rajot, J. L., Desboeufs, K., Saïd, F., Grand, N., Chevaillier, S., and Schmechtig, C.: Airborne observations  
1033 of mineral dust over western Africa in the summer Monsoon season: spatial and vertical variability of physico-  
1034 chemical and optical properties, 11, 6387–6410, <https://doi.org/10.5194/acp-11-6387-2011>, 2011.

- 1035 Formenti, P., Di Biagio, C., Huang, Y., Kok, J., Mallet, M. D., Boulanger, D., and Cazaunau, M.: Look-up tables  
1036 resolved by complex refractive index to correct particle sizes measured by common research-grade optical  
1037 particle counters, *Atmos. Meas. Tech. Discuss.* [preprint], <https://doi.org/10.5194/amt-2021-403>, in review,  
1038 2021.
- 1039 Fratini, G., Ciccioli, P., Febo, A., Forgione, A., and Valentini, R.: Size-segregated fluxes of mineral dust from a desert  
1040 area of northern China by eddy covariance, *7*, 2839–2854, <https://doi.org/10.5194/acp-7-2839-2007>, 2007.
- 1041 Gillette, D. A., Blifford, I. H., and Fenster, C. R.: Measurements of Aerosol Size Distributions and Vertical Fluxes of  
1042 Aerosols on Land Subject to Wind Erosion, *J. Appl. Meteor.*, *11*, 977–987, [https://doi.org/10.1175/1520-0450\(1972\)011<0977:MOASDA>2.0.CO;2](https://doi.org/10.1175/1520-0450(1972)011<0977:MOASDA>2.0.CO;2), 1972.
- 1044 Gillette, D.A. On the production of soil wind erosion having the potential for long range transport. *J. Rech. Atmos.*  
1045 *8*, 734–744 (1974).
- 1046 Gillette, D. A., Blifford, I. H., and Fryrear, D. W.: The influence of wind velocity on the size distributions of aerosols  
1047 generated by the wind erosion of soils, *79*, 4068–4075, <https://doi.org/10.1029/JC079i027p04068>, 1974.
- 1048 Gillette, D. A. and Nagamoto, C. 1993. Size distribution and single particle composition for two dust storms in  
1049 Soviet central Asia in September 1989 and size distribution and chemical composition of local soil. In: Joint  
1050 Soviet–American Experiment on Arid Aerosol (eds. G. S. Golitsyn, D. A. Gillette, T. Johnson, V. N. Ivanov, S. M.  
1051 Kolomiets, and co-editors). Hydrometeoizdat, St. Petersburg, 135–146.
- 1052 González-Flórez, C., Klose, M., Alastuey, A., Dupont, S., Escribano, J., Etyemezian, V., Gonzalez-Romero, A., Huang,  
1053 Y., Kandler, K., Nikolich, G., Panta, A., Querol, X., Reche, C., Yus-Díez, J., and Pérez García-Pando, C.: Insights into  
1054 the size-resolved dust emission from field measurements in the Moroccan Sahara, *Atmos. Chem. Phys.*, *23*, 7177–  
1055 7212, <https://doi.org/10.5194/acp-23-7177-2023>, 2023.
- 1056 Hinds, W. C.: *Aerosol technology: properties, behavior, and measurement of airborne particles*, John Wiley & Sons,  
1057 Chichester, 504 pp., 1999.
- 1058 Huang, Y., Kok, J. F., Martin, R. L., Swet, N., Katra, I., Gill, T. E., Reynolds, R. L., and Freire, L. S.: Fine dust emissions  
1059 from active sands at coastal Oceano Dunes, California, *19*, 2947–2964, [https://doi.org/10.5194/acp-19-2947-](https://doi.org/10.5194/acp-19-2947-2019)  
1060 2019, 2019.
- 1061 Huang, Y., Adebisi, A. A., Formenti, P., & Kok, J. F. (2021). Linking the different diameter types of aspherical desert  
1062 dust indicates that models underestimate coarse dust emission. *Geophysical Research Letters*, *48*,  
1063 e2020GL092054. <https://doi.org/10.1029/2020GL092054>
- 1064 Huang, Y., Kok, J. F., Kandler, K., Lindqvist, H., Nousiainen, T., Sakai, T., et al. (2020). Climate models and remote  
1065 sensing retrievals neglect substantial desert dust asphericity. *Geophysical Research Letters*, *47*, e2019GL086592.  
1066 <https://doi.org/10.1029/2019GL086592>
- 1067 Johnson, B. T. and Osborne, S. R.: Physical and optical properties of mineral dust aerosol measured by aircraft  
1068 during the GERBILS campaign, *137*, 1117–1130, <https://doi.org/10.1002/qj.777>, 2011.
- 1069 Jung, E., Albrecht, B., Prospero, J. M., Jonsson, H. H., and Kreidenweis, S. M.: Vertical structure of aerosols,  
1070 temperature, and moisture associated with an intense African dust event observed over the eastern Caribbean,  
1071 *Journal of Geophysical Research: Atmospheres*, *118*, 4623–4643, <https://doi.org/10.1002/jgrd.50352>, 2013.
- 1072 Kandler, K., Benker, N., Bundke, U., Cuevas, E., Ebert, M., Knippertz, P., Rodriguez, S., Schütz, L., and Weinbruch,  
1073 S.: Chemical composition and complex refractive index of Saharan mineral dust at Izana, Tenerife (Spain) derived  
1074 by electron microscopy, *Atmos. Environ.*, *41*, 8058–8074, 2007.
- 1075 Kandler, K., Schütz, L., Deutscher, C., Ebert, M., Hofmann, H., JÄCKEL, S., Jaenicke, R., Knippertz, P., Lieke, K.,  
1076 Massling, A., Petzold, A., Schladitz, A., Weinzierl, B., Wiedensohler, A., Zorn, S., and Weinbruch, S.: Size  
1077 distribution, mass concentration, chemical and mineralogical composition and derived optical parameters of the  
1078 boundary layer aerosol at Tinfou, Morocco, during SAMUM 2006, *61*, 32–50, [https://doi.org/10.1111/j.1600-](https://doi.org/10.1111/j.1600-0889.2008.00385.x)  
1079 0889.2008.00385.x, 2009.
- 1080 Kandler, K., Schütz, L., Jäckel, S., Lieke, K., Emmel, C., Müller-Ebert, D., Ebert, M., Scheuvs, D., Schladitz, A.,  
1081 Šegvić, B., Wiedensohler, A., and Weinbruch, S.: Ground-based off-line aerosol measurements at Praia, Cape  
1082 Verde, during the Saharan Mineral Dust Experiment: microphysical properties and mineralogy, *63*, 459–474,  
1083 <https://doi.org/10.1111/j.1600-0889.2011.00546.x>, 2011.

- 1084 Khalfallah, B., Bouet, C., Labiadh, M. T., Alfaro, S. C., Bergametti, G., Marticorena, B., Lafon, S., Chevaillier, S., Féron,  
1085 A., Hease, P., Tureaux, T. H. des, Sekrafi, S., Zapf, P., and Rajot, J. L.: Influence of Atmospheric Stability on the Size  
1086 Distribution of the Vertical Dust Flux Measured in Eroding Conditions Over a Flat Bare Sandy Field, 125,  
1087 e2019JD031185, <https://doi.org/10.1029/2019JD031185>, 2020.
- 1088 Kobayashi, H., Arao, K., Murayama, T., Iokibe, K., Koga, R., and Shiobara, M.: High-Resolution Measurement of Size  
1089 Distributions of Asian Dust Using a Coulter Multisizer, *J. Atmos. Oceanic Technol.*, 24, 194–205,  
1090 <https://doi.org/10.1175/JTECH1965.1>, 2007.
- 1091 Kok, J. F., Ridley, D. A., Zhou, Q., Miller, R. L., Zhao, C., Heald, C. L., Ward, D. S., Albani, S., and Haustein, K.: Smaller  
1092 desert dust cooling effect estimated from analysis of dust size and abundance, 10, 274–278,  
1093 <https://doi.org/10.1038/ngeo2912>, 2017.
- 1094 Mahowald, N., Albani, S., Kok, J. F., Engelstaeder, S., Scanza, R., Ward, D. S., and Flanner, M. G.: The size distribution  
1095 of desert dust aerosols and its impact on the Earth system, *Aeolian Research*, 15, 53–71,  
1096 doi:10.1016/j.aeolia.2013.09.002, 2014
- 1097 Maring, H., Savoie, D. L., Izaguirre, M. A., McCormick, C., Arimoto, R., Prospero, J. M., and Pilinis, C.: Aerosol  
1098 physical and optical properties and their relationship to aerosol composition in the free troposphere at Izaña,  
1099 Tenerife, Canary Islands, during July 1995, 105, 14677–14700, <https://doi.org/10.1029/2000JD900106>, 2000.
- 1100 Maring, H., Savoie, D. L., Izaguirre, M. A., Custals, L., and Reid, J. S.: Mineral dust aerosol size distribution change  
1101 during atmospheric transport, 108, <https://doi.org/10.1029/2002JD002536>, 2003.
- 1102 McConnell, C. L., Highwood, E. J., Coe, H., Formenti, P., Anderson, B., Osborne, S., Nava, S., Desboeufs, K., Chen,  
1103 G., and Harrison, M. a. J.: Seasonal variations of the physical and optical characteristics of Saharan dust: Results  
1104 from the Dust Outflow and Deposition to the Ocean (DODO) experiment, 113,  
1105 <https://doi.org/10.1029/2007JD009606>, 2008.
- 1106 Meloni, D., Junkermann, W., Sarra, A. di, Cacciani, M., Silvestri, L. D., Iorio, T. D., Estellés, V., Gómez-Amo, J. L.,  
1107 Pace, G., and Sferlazzo, D. M.: Altitude-resolved shortwave and longwave radiative effects of desert dust in the  
1108 Mediterranean during the GAMARF campaign: Indications of a net daily cooling in the dust layer, 120, 3386–3407,  
1109 <https://doi.org/10.1002/2014JD022312>, 2015.
- 1110 Mishchenko, M. I., Travis, L. D., Kahn, R. A., and West, R. A.: Modeling phase function for dustlike tropospheric  
1111 aerosols using a shape mixture of randomly oriented poly-disperse spheroids, *J. Geophys. Res.*, 102, 16831–  
1112 16847, <https://doi.org/10.1029/96JD02110>, 1997.
- 1113 Müller, K., Lehmann, S., van Pinxteren, D., Gnauk, T., Niedermeier, N., Wiedensohler, A., and Herrmann, H.: Particle  
1114 characterization at the Cape Verde atmospheric observatory during the 2007 RHaMBLe intensive, 10, 2709–2721,  
1115 <https://doi.org/10.5194/acp-10-2709-2010>, 2010.
- 1116 Osborne, S. R., Johnson, B. T., Haywood, J. M., Baran, A. J., Harrison, M. a. J., and McConnell, C. L.: Physical and  
1117 optical properties of mineral dust aerosol during the Dust and Biomass-burning Experiment, 113,  
1118 <https://doi.org/10.1029/2007JD009551>, 2008.
- 1119 Otto, S., de Reus, M., Trautmann, T., Thomas, A., Wendisch, M., and Borrmann, S.: Atmospheric radiative effects  
1120 of an in situ measured Saharan dust plume and the role of large particles, 7, 4887–4903,  
1121 <https://doi.org/10.5194/acp-7-4887-2007>, 2007.
- 1122 Quinn, P. K., Coffman, D. J., Bates, T. S., Miller, T. L., Johnson, J. E., Welton, E. J., Neusüss, C., Miller, M., and  
1123 Sheridan, P. J.: Aerosol optical properties during INDOEX 1999: Means, variability, and controlling factors, *J.*  
1124 *Geophys. Res.*, 107( D19), 8020, doi:10.1029/2000JD000037, 2002.
- 1125 Rajot, J. L., Formenti, P., Alfaro, S., Desboeufs, K., Chevaillier, S., Chatenet, B., Gaudichet, A., Journet, E.,  
1126 Marticorena, B., Triquet, S., Maman, A., Mouget, N., and Zakou, A.: AMMA dust experiment: An overview of  
1127 measurements performed during the dry season special observation period (SOP0) at the Banizoumbou (Niger)  
1128 supersite, 113, <https://doi.org/10.1029/2008JD009906>, 2008.
- 1129 Reid, E. A., Reid, J. S., Meier, M. M., Dunlap, M. R., Cliff, S. S., Broumas, A., Perry, K., and Maring, H.:  
1130 Characterization of African dust transported to Puerto Rico by individual particle and size segregated bulk analysis,  
1131 108, <https://doi.org/10.1029/2002JD002935>, 2003a.

- 1132 Reid, J. S., Jonsson, H. H., Maring, H. B., Smirnov, A., Savoie, D. L., Cliff, S. S., Reid, E. A., Livingston, J. M., Meier, M.  
 1133 M., Dubovik, O., and Tsay, S.-C.: Comparison of size and morphological measurements of coarse mode dust  
 1134 particles from Africa, 108, <https://doi.org/10.1029/2002JD002485>, 2003b.
- 1135 Reid, J. S., Reid, E. A., Walker, A., Piketh, S., Cliff, S., Mandoos, A. A., Tsay, S.-C., and Eck, T. F.: Dynamics of  
 1136 southwest Asian dust particle size characteristics with implications for global dust research, 113,  
 1137 <https://doi.org/10.1029/2007JD009752>, 2008.
- 1138 Renard, J.-B., Dulac, F., Durand, P., Bourgeois, Q., Denjean, C., Vignelles, D., Couté, B., Jeannot, M., Verdier, N.,  
 1139 and Mallet, M.: In situ measurements of desert dust particles above the western Mediterranean Sea with the  
 1140 balloon-borne Light Optical Aerosol Counter/sizer (LOAC) during the ChArMEx campaign of summer 2013, 18,  
 1141 3677–3699, <https://doi.org/10.5194/acp-18-3677-2018>, 2018.
- 1142 de Reus, M., Dentener, F., Thomas, A., Borrmann, S., Ström, J., and Lelieveld, J.: Airborne observations of dust  
 1143 aerosol over the North Atlantic Ocean during ACE 2: Indications for heterogeneous ozone destruction, 105, 15263–  
 1144 15275, <https://doi.org/10.1029/2000JD900164>, 2000.
- 1145 Rosenberg, P. D., Dean, A. R., Williams, P. I., Dorsey, J. R., Minikin, A., Pickering, M. A., and Petzold, A.: Particle  
 1146 sizing calibration with refractive index correction for light scattering optical particle counters and impacts upon  
 1147 PCASP and CDP data collected during the Fennec campaign, 5, 1147–1163, <https://doi.org/10.5194/amt-5-1147-2012>, 2012.
- 1149 Rosenberg, P. D., Parker, D. J., Ryder, C. L., Marsham, J. H., Garcia-Carreras, L., Dorsey, J. R., Brooks, I. M., Dean, A.  
 1150 R., Crosier, J., McQuaid, J. B., and Washington, R.: Quantifying particle size and turbulent scale dependence of dust  
 1151 flux in the Sahara using aircraft measurements, 119, 7577–7598, <https://doi.org/10.1002/2013JD021255>, 2014.
- 1152 Ryder, C. L., Highwood, E. J., Lai, T. M., Sodemann, H., and Marsham, J. H.: Impact of atmospheric transport on the  
 1153 evolution of microphysical and optical properties of Saharan dust, 40, 2433–2438,  
 1154 <https://doi.org/10.1002/grl.50482>, 2013a.
- 1155 Ryder, C. L., Highwood, E. J., Rosenberg, P. D., Trembath, J., Brooke, J. K., Bart, M., Dean, A., Crosier, J., Dorsey, J.,  
 1156 Brindley, H., Banks, J., Marsham, J. H., McQuaid, J. B., Sodemann, H., and Washington, R.: Optical properties of  
 1157 Saharan dust aerosol and contribution from the coarse mode as measured during the Fennec 2011 aircraft  
 1158 campaign, 13, 303–325, <https://doi.org/10.5194/acp-13-303-2013>, 2013b.
- 1159 Ryder, C. L., Marenco, F., Brooke, J. K., Estelles, V., Cotton, R., Formenti, P., McQuaid, J. B., Price, H. C., Liu, D.,  
 1160 Ausset, P., Rosenberg, P. D., Taylor, J. W., Choulaton, T., Bower, K., Coe, H., Gallagher, M., Crosier, J., Lloyd, G.,  
 1161 Highwood, E. J., and Murray, B. J.: Coarse-mode mineral dust size distributions, composition and optical properties  
 1162 from AER-D aircraft measurements over the tropical eastern Atlantic, 18, 17225–17257,  
 1163 <https://doi.org/10.5194/acp-18-17225-2018>, 2018.
- 1164 Sanchez-Marroquin, A., Hedges, D. H. P., Hiscock, M., Parker, S. T., Rosenberg, P. D., Trembath, J., Walshaw, R.,  
 1165 Burke, I. T., McQuaid, J. B., and Murray, B. J.: Characterisation of the filter inlet system on the FAAM BAe-146  
 1166 research aircraft and its use for size-resolved aerosol composition measurements, *Atmos. Meas. Tech.*, 12, 5741–  
 1167 5763, <https://doi.org/10.5194/amt-12-5741-2019>, 2019.
- 1168 Schladitz, A., Müller, T., Nowak, A., Kandler, K., Lieke, K., Massling, A., and Wiedensohler, A.: In situ aerosol  
 1169 characterization at Cape Verde, 63, 531–548, <https://doi.org/10.1111/j.1600-0889.2011.00569.x>, 2011.
- 1170 Schütz, L. and Jaenicke, R.: Particle Number and Mass Distributions above 10–4 cm Radius in Sand and Aerosol of  
 1171 the Sahara Desert, *J. Appl. Meteor.*, 13, 863–870, [https://doi.org/10.1175/1520-0450\(1974\)013<0863:PNAMDA>2.0.CO;2](https://doi.org/10.1175/1520-0450(1974)013<0863:PNAMDA>2.0.CO;2), 1974.
- 1173 Schütz, L., Jaenicke, R., and Pietrek, H.: Saharan dust transport over the North Atlantic Ocean,  
 1174 <https://doi.org/10.1130/SPE186-p87>, 1981.
- 1175 Shao, Y., Ishizuka, M., Mikami, M., and Leys, J. F.: Parameterization of size-resolved dust emission and validation  
 1176 with measurements, 116, <https://doi.org/10.1029/2010JD014527>, 2011.
- 1177 Sow, M., Alfaro, S. C., Rajot, J. L., and Marticorena, B.: Size resolved dust emission fluxes measured in Niger during  
 1178 3 dust storms of the AMMA experiment, 9, 3881–3891, <https://doi.org/10.5194/acp-9-3881-2009>, 2009.

- 1179 Struckmeier, C., Drewnick, F., Fachinger, F., Gobbi, G. P., and Borrmann, S.: Atmospheric aerosols in Rome, Italy:  
1180 sources, dynamics and spatial variations during two seasons, 16, 15277–15299, [https://doi.org/10.5194/acp-16-](https://doi.org/10.5194/acp-16-15277-2016)  
1181 15277–2016, 2016.
- 1182 Sviridenkov, M. A., Gillette, D. A., Isakov, A. A., Sokolik, I. N., Smirnov, V. V., Belan, B. D., Pachenko, M. V.,  
1183 Andronova, A. V., Kolomiets, S. M., Zhukov, V. M., and Zhukovsky, D. A.: Size distributions of dust aerosol measured  
1184 during the Soviet–American experiment in Tadjikistan, 1989, *Atmospheric Environment. Part A. General Topics*,  
1185 27, 2481–2486, [https://doi.org/10.1016/0960-1686\(93\)90019-U](https://doi.org/10.1016/0960-1686(93)90019-U), 1993.
- 1186 Wagner, F., Bortoli, D., Pereira, S., Costa, M. Jo., Silva, A. M., Weinzierl, B., Esselborn, M., Petzold, A., Rasp, K.,  
1187 Heinold, B., and Tegen, I.: Properties of dust aerosol particles transported to Portugal from the Sahara desert, 61,  
1188 297–306, <https://doi.org/10.1111/j.1600-0889.2008.00393.x>, 2009.
- 1189 Walser, A., Sauer, D., Spanu, A., Gasteiger, J., and Weinzierl, B.: On the parametrization of optical particle counter  
1190 response including instrument–induced broadening of size spectra and a self–consistent evaluation of calibration  
1191 measurements, 10, 4341–4361, <https://doi.org/10.5194/amt-10-4341-2017>, 2017.
- 1192 Wendisch, M., and J.–L. Brenguier, *Airborne Measurements for Environmental Research*, Wiley–VCH., 2013
- 1193 Weinzierl, B., Petzold, A., Esselborn, M., Wirth, M., Rasp, K., Kandler, K., SchütZ, L., Koepke, P., and Fiebig, M.:  
1194 Airborne measurements of dust layer properties, particle size distribution and mixing state of Saharan dust during  
1195 SAMUM 2006, 61, 96–117, <https://doi.org/10.1111/j.1600-0889.2008.00392.x>, 2009.
- 1196 Weinzierl, B., Sauer, D., Esselborn, M., Petzold, A., Veira, A., Rose, M., Mund, S., Wirth, M., Ansmann, A., Tesche,  
1197 M., Gross, S., and Freudenthaler, V.: Microphysical and optical properties of dust and tropical biomass burning  
1198 aerosol layers in the Cape Verde region—an overview of the airborne in situ and lidar measurements during  
1199 SAMUM–2, 63, 589–618, <https://doi.org/10.1111/j.1600-0889.2011.00566.x>, 2011.
- 1200 Weinzierl, B., Ansmann, A., Prospero, J. M., Althausen, D., Benker, N., Chouza, F., Dollner, M., Farrell, D., Fomba,  
1201 W. K., Freudenthaler, V., Gasteiger, J., Groß, S., Haarig, M., Heinold, B., Kandler, K., Kristensen, T. B., Mayol–  
1202 Bracero, O. L., Müller, T., Reitebuch, O., Sauer, D., Schäfler, A., Schepanski, K., Spanu, A., Tegen, I., Toledano, C.,  
1203 and Walser, A.: The Saharan Aerosol Long–Range Transport and Aerosol–Cloud–Interaction Experiment: Overview  
1204 and Selected Highlights, *Bull. Amer. Meteor. Soc.*, 98, 1427–1451, <https://doi.org/10.1175/BAMS-D-15-00142.1>,  
1205 2017.
- 1206